NASA CONTRACTOR REPORT

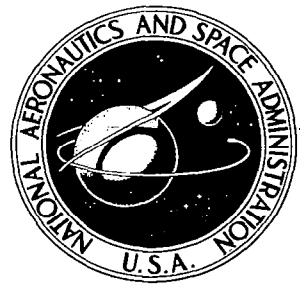

ANALYSIS OF LUNA 9 PHOTOGRAPHY

Prepared by
LOCKHEED ELECTRONICS COMPANY
Houston, Texas
for Manned Spacecraft Center

NATIONAL AERONAUTICS AND SPACE ADMINISTRATION • WASHINGTON, D. C. • FEBRUARY 1968

ANALYSIS OF LUNA 9 PHOTOGRAPHY

Issued by Originator as LEC/HASD Report No. 671-40-019

Prepared under Contract No. NAS 9-5191 by
LOCKHEED ELECTRONICS COMPANY
Houston, Texas

for Manned Spacecraft Center

NATIONAL AERONAUTICS AND SPACE ADMINISTRATION

For sale by the Clearinghouse for Federal Scientific and Technical Information
Springfield, Virginia 22151 – CFSTI price $3.00

ABSTRACT

As a means of acquiring additional information about the Moon and the environment at its surface, the Mapping Sciences Branch (MSB), under the requirement of NASA/MSC, has conducted a detailed scientific evaluation and analysis of Luna 9 spacecraft imagery.

Presented in this report are the techniques and procedures used for this study, and the results with the conclusions drawn.

The first section of the report discusses the nature and specifications of the spacecraft and its instruments. Included here also are the image transmissions and images received.

In the second section, detailed descriptions of the image frames are given. These include: scale and panoramic coverage of the frames, azimuth and distances of the image features, size and classification of the surface materials, and size and classification of the visible craters.

The third section discusses the procedures and techniques used for the above calculations. These are discussed as applied to monoscopic panoramas, dihedral mirror images, and stereoscopic panoramas.

From the results of this investigation, the following conclusions have been drawn: (1) the Luna 9 vehicle contained a simple panoramic camera mechanism which telemetered photographic panoramas of the lunar landscape. (2) The spacecraft made a soft landing inside and near the edge of a crater which is elliptical in diameter measurements. Since the rim of this crater is higher than the area where the spacecraft landed, the field of its camera system was confined to a specific local environment. (3) The surface materials in this area consist of a highly vesicular to frothy bedrock, with scattered particles up to cobble size which are unevenly distributed over the surface. (5) Craters which are visible range in size from 15 meters in diameter to those barely visible. (6) Although a more sophisticated method of reduction with better quality imagery will furnish more precise results, it will not improve the relative accuracy of the results presented here.

Considerably more work remains to be done on the reduction of the Luna 9 images, both qualitative and quantitative. The results presented here are not a complete evaluation of the imagery available; however, they do represent the summation of considerable effort in evaluation and technique. Erroneous premises and assumptions have been disproven and eliminated where possible. It is hoped that the findings of this report will serve as a guide for further investigation.

TABLE OF CONTENTS

TABLE OF CONTENTS (CONT'D)

TABLE OF CONTENTS (CONT'D)

TABLE OF CONTENTS (CONT'D)

LIST OF TABLES

SECTION 1

INTRODUCTION

1.1 GENERAL COMMENTS

Since the soft-landing of the Luna 9 spacecraft on the moon's surface on February 3, 1966, its soft landing; picture data transmission; and imagery transmitted have created much interest and study.

Early in February, Russian press releases of the Luna 9 imagery were made available. These were transmitted by the Associated Press and distributed in the form of wire photos consisting of portions of the panoramic scene transmitted from the spacecraft.

At the MSC, under the requirements of NASA/MSC, these panoramas have received detailed scientific evaluation and analysis by the Mapping Sciences Branch (MSB).

In this report the techniques and procedures used for this study, and the results with the conclusions drawn are presented. These are categorized and discussed as follows:

Section I - Nature and specifications of the spacecraft and its instruments (with a more specific analysis of the camera system); type of image transmission;

and images received.

Section II - Detailed descriptions of the image frames, including: scale and panoramic coverage; azimuth and distances of the image features; size and classification of the surface materials; and size and classification of the visible craters.

Section III - Discussion of the procedures and techniques for the above calculations. These are discussed as applied to monoscopic panoramas, dihedral mirror images, and stereoscopic panoramas.

Although the simplest mathematical principles have been used, vector analysis and more advanced mathematical techniques may provide a more sophisticated solution, however, this will not improve the relative accuracy of the results presented here.

1.2 THE VEHICLE

The nature and specifications of the spacecraft launched by the Russians has received widespread attention. Details have been deduced by various means and considerable information has been released by the Russians. Its design is simple but effective.

Of primary interest to MSB is the portion of the spacecraft which transmitted the picture data to earth. Figure 1 shows the first sketch of the instrument released by the Russians shortly after the February landing. Figures 2 and 3 show two photographs of the spacecraft released in Vienna at the International Space Symposium in mid-May, 1966. A brief description of the salient features of the capsule is given below.

The capsule is spherical in shape, approximately 60 cm (24 inches) in diameter. The upper hemisphere is divided into four sections or "petals". These sections protect the scanning mechanisms and other delicate parts of the spacecraft. They opened - probably on command - after the capsule had come to rest in an inclined position. The amount of control over the inclination and orientation of the tilt axis is purely a matter of conjecture at this time.

Upon command, the four petals (viewed in Figures 2 and 3) opened by means of a latch release mechanism. The four antennas, inclined outward from the spacecraft vertical axis, could probably be extended on command. Spade-shaped colorimetric or photometric charts are attached to the ends of the antennas by means of a thin wire or cord. These also serve

as plumbs for defining the true vertical.

Spaced between the antennas are three dihedral mirrors. Two mirrors are 180° apart, with the third placed slightly off the midpoint of the first two.

Other instrumentation is seen on the photographs of Figures 2 and 3 and in the images received. The functions of these are not known, but are presumed to be magnetic and radiation detectors, or other sensing devices.

1.3 NATURE OF IMAGES

1.3.1 TYPE OF IMAGE TRANSMISSION. The "camera" is housed in a small cylindrical protuberance on the top of the capsule. This is, apparently, a simple facsimile camera functioning in a manner shown in the sketch below.

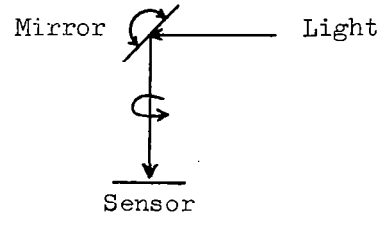

It consists of a small mirror nutating about a horizontal axis, and capable of rotating 360° about the camera vertical. The vertical angle scanned was about 30°, 15° above and below the camera horizontal. The image was probably transmitted concurrently with the scan.

The instrument scanned about 6000 vertical lines per 360° revolution,

which reportedly took one hour. The scan line width was thus approximately 1/1000th of a radian (milliradian) and may be considered the resolving power of the system.

1.3.2 IMAGE TRANSMISSION TIME. There were five transmissions from the Luna 9 spacecraft. The first was a partial scan taken some $4\frac{1}{2}$ minutes after the landing. The last was taken on February 6, three days after the landing. Since neither of these two transmissions were made available and they are reportedly of poor quality, they will not be considered further. The remaining three panoramas were transmitted on the 4th and 5th of February. Table 1 is a summary of the transmission time, the approximate scan elevation, and the amount of tilt of the spacecraft as interpreted in this paper.

TABLE 1. IMAGE TRANSMISSION TIME OF LUNA 9 PANORAMAS

Transmission	Tilt of Capsule	Approximate Time	Date	Approximate Sun Elevation
1st Panorama	13°	01:50-3:30 UT	Feb. 4	7°-8°
2nd Panorama	16°-18°(?)	15:30-17:10 UT	Feb. 4	14°-15°
3rd Panorama	21°-23°	16:00-17:40 UT	Feb. 5	26.5°-27.5°

Only portions of these three panoramas were available for study in the Associated Press news wire photo releases. These were eleven frames of varying size, no combination of which would make a full panorama and most of which were of the third panorama. Table 2 shows the number

of frames from each panorama, and the coverage width in degrees with the reference point or 0° orientation taken as the line of greatest inclination or tilt of the camera system. This reference point is common throughout this report. For convenience, the frames are labeled alphabetically from left to right. A subscript number is used to designate the scan to which the frame belongs, e.g., A_3 is the left frame of the third panorama, etc..

TABLE 2. NUMBER AND COVERAGE OF LUNA 9 TRANSMISSIONS

FRAME	A	B	C	D	E	F	G
1st Panorama	238°-298°		-	-	-	55°-100°	100°-144°
2nd Panorama	-	262°-305°	-	-	-	-	-
3rd Panorama	238°-262°	262°-305°	307°-330°	330°-10°	15°-60°	60°-98°	103°-151°

It will be noted from the table that there are gaps between frames, even in the third panorama. This made it somewhat difficult to place the images in their proper position, however, the image orientation, as seen in Table 2, was accomplished through a study of the camera instrumentation, as seen in the imagery, and topographic details in landscape. For orientation of the full panorama, reference may be made to panoramic sketch of Figure 4 which was reconstructed from the frames of the third panoramic scan.

As shown in Table 2, only the horizon photographs to the left and right were available from the first panorama. The single photograph of the second panorama is of questionable authenticity, since it seems to be

an exact duplicate of its counterpart in the third panoramic scan. The most complete coverage is in the third panorama which is also incomplete (short by 94°).

None of the available frames covered the reverse (180°) portion of the lunar scene. Details of this part of the scan were taken from published news releases.

Table 3 lists the frame identification letter and number as used in this report, with its corresponding A.P. news release number and the NASA-MSC Photographic Laboratory number.

TABLE 3. INDEX OF PHOTOGRAPHS OF LUNA 9 TRANSMISSIONS

Frame Identification Letter and Number This Report	A.P. News Release Number and Date	MSC Number
A_1B_1	N.Y. 12, Feb. 6, 1966	S-66-20041
F_1	N.Y. 31, Feb. 5, 1966	S-66-20039
G_1	N.Y. 31, Feb. 5, 1966	S-66-20040
B_2	N.Y. 24, Feb. 7, 1966	S-66-20044 S-66-20045
A_3	N.Y. 31, Feb. 7, 1966	S-66-20046
B_3	N.Y. 31, Feb. 7, 1966	S-66-20046 S-66-20047
C_3	N.Y. 31, Feb. 7, 1966	S-66-20047
D_3	N.Y. 32, Feb. 7, 1966	S-66-20042

Table 3.
(cont'd)

Frame Identification Letter and Number This Report	A.P. News Release Number and Date	MSC Number
E_3	N.Y. 32, Feb. 7, 1966	S-66-20043
F_3	N.Y. 33, Feb. 7, 1966	S-66-20038
G_3	N.Y. 33, Feb. 7, 1966	S-66-20037

SECTION 2

DESCRIPTION OF IMAGERY

The following description of the image frames received is based primarily on the third panorama, which is the most complete. Deviations in the imagery based on frames from the first panorama are also noted. Copies of all the frames, with annotation overlays, are presented in Figures 5 through 15. For a view of the complete panorama, reference may be made to Figure 4, which is a perspective sketch of the third panorama. Quantitative information mentioned in the descriptions were derived by methods outlined in Section 3 below.

2.1 FRAME A (Figures 5 and 13)

This frame includes about 24° (238°-262°) of the left end of the panorama. The sky covers most of the frame. The latch mechanism and petal obscures much of the lunar landscape. The horizon to the left of the petal is about 170 meters distance. To the right of the petal, the sloping edge of a small crater obscures the true horizon. The latch is reportedly 8 cm in diameter. Its image size would, therefore, indicate a distance of about 80 cm from the camera to the petal when fully extended.

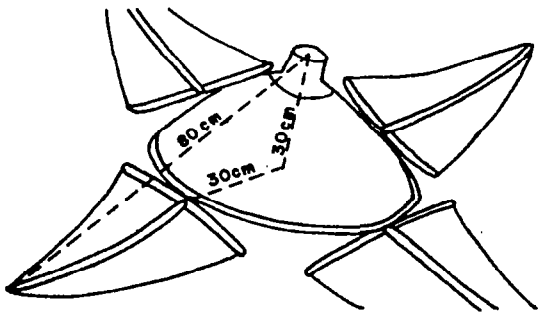

In the first panorama of the same area (shown in the left part of Figure 13) the latch mechanism is below the horizon, giving a fuller view. The horizon is obscured by shadows on the left side of the crater, indicating a local slope of 7° or 8°. The small promontory on the horizon is important in this view, since it is one of the mirror images reflected in a dihedral mirror, and is obscured by the petal mechanism on the third panorama.

The scale on the horizon in Frame A is about 1:600 to the left of the petal, and about 1:35 on the slope of the crater to the right of the petal.

As the spacecraft tilted to a greater angle (approx. 9°), the difference in the image size and position of the petal (Figures 5 and 13) indicates that the petal was forced upwards towards the camera; and, therefore, suggests that the petal was in contact with the lunar surface. This condition also corresponds with the position of the petal seen in Frame F, discussed below.

2.2 FRAME B (Figures 6, 12, and 13)

This frame matches the left edge of Frame A and covers about 43° of angular view.

Its most prominent feature is the instrument in the center of the field. It occupies the position of an antenna which can be seen in Figure 2,

however, which is not visible in any of the panoramas. The function of the instrument is not known.

The frame exhibits a fairly complete view of the horizon on the right half of the frame. Horizon distance here is 70 to 95 meters (scales 1:233 - 1:320). Distance to the ground at the lower right hand corner is about 1.5 meters (scale 1:5). Several scattered angular rocks are seen in the foregound, the largest of which is about 15 cm. (6 inches) in maximum diameter. The rock protruding above the horizon at 290° is about 70 cm. (30 inches) high.

Near the lower right portion of the instrument is a small irregular scarp. This scarp is apparently continuous behind the instrument and below the field of view. It also continues on to the left as shown in the panoramic sketch (Figure 4). These details show more clearly in Frame A_1B_1 of the first panorama (Figure 13).

To the left of the instrument, the view is foreshortened by a small crater. The center of this crater is about 20 meters (60 feet) from the camera with a diameter of about 12 meters (36 feet). Its minimum depth is 0.5 meters (1.6 feet).

Frame B_2, supposedly taken on the second panorama, is shown in Figure 12. It is identical in all respects to Frame B_3, even to shadow detail. It is concluded here that the original release was in error, and that the second-scan photographs are in reality identical to the third panorama imagery.

The details of the Frame B section of the panorama are more clearly seen in Frame A_1B_1 (Figure 13). This is due to the effect of a lower sun elevation on the photography. Immediately to the left of the instrument, at 277°, is a marked interruption of the imagery appearing similar to a mirror image. A closer inspection, however, determined that this discontinuity was apparently caused by a malfunction in the telemetry system.

2.3 FRAME C (Figure 7)

There is a small 2° strip missing between Frame B and C. Frame C has an angular coverage of 23°. This is a low-oblique, close-up view of the surface. Distance to the images in the upper left hand corner is 5-6 meters (scale 1:20) to the lower right hand corner, about 1 meter (scale 1:33). The first of three dihedral mirrors present in the scan is seen at 315° (image azimuth refers to notations at top of figure). The mirrors are numbered in sequence from the left. Those in this frame are nos. 1 (on the left) and 2 (on the right). Mirror no. 1 reflects the surface near the spacecraft to the right. These reflected areas are outlined in Figure 4 and may be identified by their primed numbers.

Near the top of mirror 2, the reflected image is masked by a dark object extending diagonally across the mirror. This is apparently the antenna at 12°30' which is canted outward from the camera axis.

The mirrors show marked asymmetry, i.e., the mirror on the left (no. 1) shows a much narrower face than that on the right (no. 2). This

immediately suggests an asymmetric orientation. The geometry of the mirrors will be discussed further in paragraph 3.2.

The lunar surface shown in Frame C_3 is pock-marked by craterlets in the upper portion. The surface is rough and irregular on a small scale. A number of discrete pebbles (largest in the left-center is about 4 centimeters in longest diameter) may be seen in the view. Smallest particle size discernible is approximately 3 mm. (1/8 inch).

2.4 FRAME D (Figure 8)

This is the center of the panorama and includes the largest scale close-up view of the lunar surface. Coverage is from 330° to 10° - a total of 40°. At the bottom center of the frame is what appears to be a sensor which is in contact with the surface and casts a shadow. This sensor occupies the position of a petal which is not visible, and apparently is too low to be included in the camera view.

In this frame, the distance is approximately 2 meters from the camera to the top center of the image, and .5 meters from the camera to the bottom center. Scales at the points are 1:7 and 1:1.7, respectively. Smallest particle size discernible in this view is about 1 mm. (0.03 inch).

At the upper right corner of the frame is the solar glare from the surface of the moon. The line of lowest inclination was within 10° of the sun direction, suggesting that some control mechanism was used for orienting the spacecraft in a solar direction.

Since this frame is larger in scale, the number of discrete rock particles seen on the surface appear to be fewer in number. The surface on which these lie is very irregular and aphanitic with a texture similar to vesvesicular basalt or scoria.

Four small craterlets may be seen in the frame - two in the left foreground, one below the top left center, and one at the top right center. These have diameters of about 15 centimeters (6 inches). The whole surface slopes gently to the right, and away from the camera, suggesting that the capsule is on the edge of a small depression or crater.

2.5 FRAME E (Figure 9)

Between Frames D and E is a missing 5° strip. This missing portion is occupied by an antenna and was probably intentionally omitted in the press releases. Frame E has an angular coverage of 45°: from 15° to 60°.

At 30° is the center of a second dihedral mirrors (nos. 3 and 4, on the left and right, respectively). There is asymmetry between the left and right mirrors, as in mirrors nos. 1 and 2. This asymmetry is due to malfunction of the telemetry system as some of the lowermost images of the left mirror (no. 3) are superimposed on the images from the right mirror (no. 4).

Mirror no. 3 reflects a close-up view of the lunar surface at about 305° to 312°, immediately to the left of the first dihedral mirrors.

Mirror no. 4 reflects the horizon to the right between the two craters at about 120°. The upper portion of this mirror shows the black sky, except for a small, white triangular portion at the top. This triangle is the reflection of the sunlit portion of the antenna at 100°.

Distance is about 5 meters (scale 1:17) to the upper right-hand corner of the frame, and about .5 meters (scale 1:1.7) to the lower left-hand corner.

Several large rock fragments are visible in the frame. These are somewhat larger than those in Frame D_3. The large broken fragment near the top right corner is about 30 centimeters long and 12 centimeters high (12 x 5 inches); the triangular fragment at the center of the left edge is 6 centimeters wide and 2.5 centimeters high (2.5 x 1 inch).

There are a number of small craterlets or depressions in the portion of the frame to the right of the mirrors. These range in size from 5 centimeters, 10 centimeters, and 15 centimeters in diameter (2, 4, and 6 inches). The largest is at the right center at coordinates 50°, 0°.

Linear features (interpreted as veins, dikes, etc., in recent public releases) may be seen in this portion of the frame. One especially prominent linear cuts across the upper side of the craterlet at coordinates 47°, -7°.

To the left of the dihedral mirrors, the surface slopes to the left and away from the spacecraft, somewhat more abruptly than in Frame D.

2.6 FRAME F (Figures 10 and 14)

Frame F_3 joins E_3 at 60° and extends to 98°, giving angular coverage of 38°. The horizon may again be seen in the upper right portion. Frame F_1, from the first panorama, covers a slightly larger area from 55° to 100°, a total of 45°.

The second of the two spacecraft petals visible in the panorama is found at the bottom of the F frames at an image azimuth of 70°. On F_1, the petal is barely visible, while on the third more steeply dipping scan, the petal is more fully exposed. This corresponds with the condition in Frame A (180° opposed), which indicates that the petal was forced upward by the lunar surface when the tilt increased.

On F_3, distances to the horizon are: 76 meters at 70° at the top of the frame (scale 1:253) and 90 meters at the right edge of the frame (scale 1:300). The foreground in the bottom left corner is about 1 meter distance from the camera (scale 1:3.4).

Just above the petal image, at (58°, -2°), is a large object which casts a shadow in both F_1 and F_3. This object has been called a rock in both Russian and U.S. press releases. The regularity of the outline of the object, and its high reflectance, leads to the inference that it is metallic, and could possibly be a mechanical portion of the spacecraft used in the soft landing. The object is about 25 centimeters (10 inches) in length and 10 centimeters (4 inches) in diameter.

The same remarks may be made of the object near the top of the frame at coordinates 72°, +9°. This appears to be a portion of a sphere suggestive of the pressurization tanks attached to the original vehicle. This object is about 16 centimeters (7 inches) radius, which would correspond to the radius of such a sphere.

There are a number of other smaller objects in the background which have a similar high specular reflectance. There is a bright glare at the bottom left in Frame F_1 (an area not seen in F_3), which indicates an object with very high reflective power.

Microdensitometer scans were made over these several objects in the fore- and background to determine if their reflectance was distinctive. The quality of the imagery and the degradation from the original was so great, that the results were inconclusive. It is suggestive, however, that the brightness level of all the objects scanned are fairly constant throughout the frame.

The lunar surface in this frame generally resembles that of the preceding views, however, this area appears slightly more frothy. A number of crater and craterlets are visible. These are more pronounced in Frame F_1 when the sun angle was much lower. Most of the small craterlets do not have rims. The largest crater, near the horizon (between 60° and 80°), is about 4 meters (12 feet) in diameter and seems to be continuous with a second crater which is not fully discernible. A few angular fragments of 0.5 to 1 meter in diameter are seen on the flanks of the crater in the earlier scan. A small funnel-shaped crater is present at coordinates 72°, +4°.

A few lineations may be seen in the Frame F_1 (Figure 14). A pair of these begin at the left edge of the frame at -8°, and extend in a diagonal direction behind the large object in the foregound.

2.7 FRAME G (Figures 11 and 15)

There is a 5° portion of the panorama missing on the left edge of Frame G_3. This gap is occupied by an antenna. The missing section may be seen in Frame G_1. Only a very small segment of the antenna may be seen in G_3 at the bottom left corner.

Figure G_3 has an angular coverage of 48°, from 103° to 151°. Frame G_1 extends from 100° to 144°. As in Frame F, some details are shown more clearly on the earlier scan (G_1) than in the later panorama.

At 135° are the third dihedral mirrors, located at 180° from the first. These mirrors are more distinct than the other two pair and present a distinctly symmetrical orientation.

The left mirror (no. 5) reflects a close-up view of the lunar surface to the left. On Frame G_3 the antenna at 102°30' sharply masks the top-most portion of the mirror image. On Frame G_1 the image is not obscured.

The right mirror in both scans reflects the sky and is predominately black. Near the bottom of both images is an odd-shaped white object. This is interpreted as a side view of a portion on the petal that should be present at about 168°, and is not directly seen in any of the scans.

Distances to the horizon are 149 meters at the lower right corner (scale 1:500), and 94 meters at the center of the left edge (scale 1:310). The distance to the nearest surface in the lower left-hand corner is about 2.5 meters (scale 1:8).

A small escarpment extends vertically across the left-hand portion of the frame, immediately adjacent to the antenna. It shows a distinct irregularity on the horizon, where it is about 1 meter in height.

The surface appeared more coarsely textured and "rubby" to the right of the scarp face than in the preceeding frames.

Two prominent craters are seen in this frame. The largest appears behind the dihedral mirror. The center of the crater is about 15 meters (50 feet) from the camera station, and is about 6 meters (20 feet) in diameter. The crater has a low rim around its perimeter.

The second crater is near the horizon between 110° and 120° in both figures. The center is about 30 meters from the camera, with a diameter of 4.6 meters (15 feet).

There are several smaller craterlets in the foreground. These are about 15 centimeters (6 inches) in diameter and smaller.

The surface near the right side of the frame (between 140° and 150°) becomes featureless because of the high reflectance, or backscatter, from the sun.

SECTION 3

GEOMETRY OF THE IMAGERY

In the descriptions of the preceeding section, distances and sizes of objects were mentioned. The methods by which these were derived are the subject of this section. These methods are discussed separately under: (1) single panorama, (2) dihedral mirrors, and (3) stereoscopic pairs. In actual practice, these three subjective divisions are mutually independent.

Future work, using better imagery, may be more successful by using more elaborate mathematical reduction methods and instrumentation. For the immediate purpose, however, the simplest mathematical methods, both computational and graphic, are deemed sufficient. Measurements were made with single scales and protractors. Calculation are to slide rule accuracy.

3.1 SINGLE PANORAMAS

Shortly after the receipt of the imagery released by the Soviets, it became evident that the Luna 9 photography was a continuous panorama, rather than a frame camera.

This difference from standard frame camera photography, which yields a perspective projection, made the geometric reduction of the Luna 9 imagery more difficult. For this work, classic photogrammetric principles, based on perspective projection, had to be modified for application to panoramic or cylindrical type projection.

Assuming that the surface as represented by the horizon is truly flat, the geometric analogy is a cylinder cut by a plane, as shown in Figure 16.

If the cylinder is vertical and the plane horizontal (i.e., the plane is perpendicular to the axis of the cylinder), the intersection will be a circle (Figure 16A). If the cylinder is cut and rolled flat, the developed line of intersection will be a straight line perpendicular to the projected axis of the cylinder. If the origin is taken as the intersection of the plane and the axis of the cylinder, the developed intersection line will coincide with the horizontal abscissa. If the origin is above or below the plane-axis intersection, the developed circle will be a straight line above or below, and parallel to the abscissa.

If the plane of intersection is at an angle to the axis of the cylinder (i.e., the cylinder is tilted with respect to the plane), the line of intersection will be an ellipse (Figure 16B). If the cylinder is cut along a line parallel to the axis, the developed intersection will be a cosine curve (or sine curve, depending on the origin selected). Again, the developed curve may move up or down the vertical ordinate line if the camera is above or below the selected origin. The curve is defined by the function of the angle of inclination, and the cylindrical (or azimuth) angle. This relation is given by the formula,

$$y = \tan \theta \cos x$$

where y is the ordinate; θ is the angle of inclination; and x is the azimuth angle in radians.

The angle of tilt (θ) is the acute angle between the tangent to the curve, where it crosses the abscissa (or center line) and the abscissa itself, as shown in Figure 16B.

The horizon curve, as seen on the panoramas, is a smooth mathematical curve resembling the one described above. Local irregularities are easily recognized. In order to make quantitative measurements on the imagery, it is necessary to determine: (1) the radius of the cylinder (or effective focal length of the camera system); (2) the tilt of the axis from the vertical; (3) the height of the camera above or below the surface; and (4) a scale factor between the images and true physical space. The methods by which these were determined, and deviations from the theoretical model above, are discussed in the following sections.

3.1.1 FOCAL LENGTH. The determination of the effective focal length of the image system may be most easily accomplished by measuring a complete panorama, which gives the circumference of the cylinder. The radius, or effective focal length, is directly obtained by the standard formula,

$$r = \frac{c}{2\pi}$$

where c is the circumference and r is the radius.

Since a full panorama was not available, it was necessary to make a plot of the instrumentation imaged in the panorama, and project circular arcs

into a full 360° circle. Figure 17 is a plan view of the results of this endeavor, with later corrections. This figure also shows the mirror image directions, which later proved useful in making angular measurements for detailed determinations.

A press release from Moscow, made available at a subsequent date, contained a full panorama, which verified the results obtained by this method.

Since the effective focal length will vary, depending upon the amount of enlargement (or reduction) of the image, a graph of the focal length versus the vertical width of the image was made for determining this variation. This graph is shown in Figure 18. Using the graph, the effective focal length for a width of 6.25 inches is 11.54 inches (294 mm) with the vertical width being about 30° in angular measure (1.8464 radians). The circumference at this scale is 72.5 inches.

Further verification of the focal length was obtained by checking the size of objects imaged in the panorama, whose dimensions were given by the Russians. The latch noted above in the comments on Frame A (section 2.1) is an example. This method is not an independent solution, since the distance to the object must also be known.

3.1.2 HEIGHT OF CAMERA. The height of camera station above the lunar surface on which it rests is established by the size of the spacecraft. Since the camera system is at the top of the spherical pod, see Figures 1,

2, and 3, the height of the camera system is the diameter of the spacecraft: 60 centimeters. The true height will be slightly less, due to the tilt of the system, i.e., about 56 to 58 centimeters. Sixty centimeters is used to simplify the calculations, except where the true value is critical.

3.1.3 RESOLUTION. In section 1.3.1, it was noted that the resolving power of the original telemetry data was 1 milliradian. On the photography used in this study, photometric investigation established a degradation of the original imagery as being 2 x. The resolution of the photography on hand is thus estimated at 2 milliradians.

The largest scale used in these studies was 6.25 inches in width or an effective focal length of 11.54 inches. The resolution at this scale is about .02 inches (.6 mm).

This resolving power of the imagery establishes a limitation on the accuracy of distance measurement. Due to the curvature of the moon, the maximum distance seen from a point 60 centimeters above a level surface is 1400(±) meters.

The apparent horizon will be the same as the true horizon at this distance. However, the resolving power of the photography limits this horizon distance. The ratio of the height to the distance will be the angle of resolution in radians as shown in the sketch below,

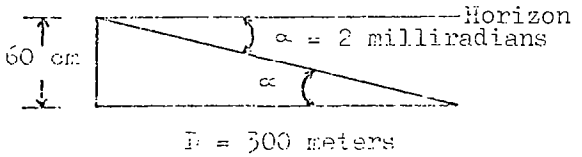

so that,

$$\frac{60 \text{ cm}}{D} = .002 \text{ radians}$$

$$D = \frac{60}{.002}$$

$$= 300 \text{ meters}$$

The maximum distance distinguishable on the photography is thus some 300 meters, i.e., any distance greater than 300 meters may be considered as infinite for purposes of measurement or distance discrimination.

3.1.4 TILT DETERMINATION. As noted in Figure 16 and the discussion in section 3.1, the tilt of a cylinder (the pancrama) intersected by horizontal plane (the horizon) may be determined at the intersection of the developed cylinder and the center line or abscissa. The angle between the abscissa and the tangent to the developed curve is the angle of tilt. This intersection is at 90° from the maximum amplitude of the curve.

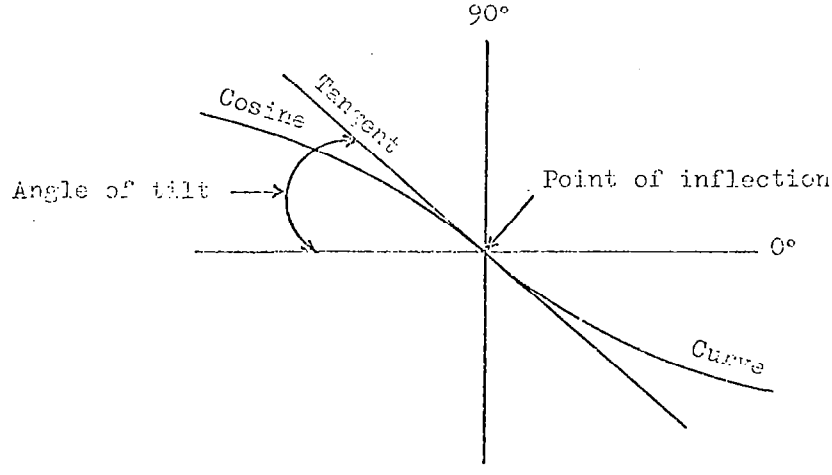

From inspection of the panorama, it may be seen that the abscissa at 90° is well below the horizon line. Further consideration of the nature of the horizon curve is necessary to account for this disparity.

Four conditions that will affect the nature of the developed horizon curve are shown in Figure 19.

In Figure 19a, the curve is affected by an increase in tilt. This causes an increase in the amplitude of the curve. The curve, however, maintains its symmetry with respect to both x and y axis.

In Figure 19b, the curve is displaced by the perspective center being below the horizon. The same effect is obtained by placing the perspective center above the horizon, as in aerial photography. In the latter case, the displacement is negative. The displacement is constant throughout the length of the curve and perpendicular to the original horizon line. Symmetry is maintained, although the line of symmetry is displaced from the abscissa.

In Figure 19c, a similar situation exists, except that the perspective center is asymmetric to the horizon, i.e., displaced from the center. The geometric analogy is the case of an oblique cone, the apex of which is the perspective center, and the cone base is the horizon line. The developed curve is asymmetric to the abscissa, displacement being perpendicular to the original horizon. Displacement is greatest at the nearest point, decreasing gradually to points where the modified and original horizons coincide.

In Figure 19d, the condition of 19c exists, with the axis of tilt at an angle to the radius from the crater center. The effect is a shifting of the horizon curve to the left or right, making the curve asymmetric to the y axis.

From inspection of the panoramas, the case of 19d corresponds to that on the Luna 9 panorama. The curve of the horizon on the imagery is assymmetric to both the x axis and y axis.

To measure the amount of tilt, it is necessary to drop a perpendicular to the horizon curve from the 90° or 270° distance on the abscissa. The tangent at this point on the abscissa is the angle of tilt of the panorama. This may also be done by finding the inflection point or point of maximum slope of the curve, either analytically or graphically. The inflection point would be the point of tangency at which the tilt is to be measured.

The results of the tilt measurements on available photographs are shown in Table 1. Further confirmation of the tilt may be obtained from the position of the minimum point of the horizon curve on the first panorama. This corresponds to a tilt of 13°, similar to that measured by the method described above.

3.1.5 DISTANCE DETERMINATIONS. It is necessary to have some known distance in the image to provide scale for measurement. Two independent lines of known distances are obtained from mirror images. The method of reduction of the mirror images is discussed in the Section 3.2. The results of the distance measurements along the mirror images are critical

for complete reduction of the panoramas.

Two lines along which mirror image measurements are possible are shown in the sketch of Figure 4. Each is independent of the other, and so provide a cross check on the accuracy. The first line, from mirror 3, is between 300° and 315°, the second line is a double line, from mirrors 2 and 5, between 45° and 60°. The distances measured between 300° to 315° are least reliable because of interruptions of the horizon by near features.

The distances were computed for individual points along the two lines. Results of the distances thus determined are shown in Table 4.

Where the horizon fell outside the imagery, the points could not be measured continuously to the horizon. To extrapolate these distances to the horizon, the lines were plotted on logarithmic paper as shown in Figure 20. The effective horizon distance is taken as 0.5 mm, the measuring accuracy being approximately equal to a resolution limit of 2 milliradians at a photo width of 6.25 inches.

The horizon distances thus determined are 66 meters for the left view at 306°, and 70 meters for the right view at 57°. These distances are inclined distances and not true horizon distances.

The calculation of additional distances on the horizon require some knowledge of the depth of the camera station below the rim of the crater. This is obtained by measuring the angle between the true and apparent horizon line, and solving the equation of the sketch on page 30.

TABLE 4. MIRROR IMAGE CALCULATIONS

Mirror No.	Point No.	α (°)	β (°)	γ (°)	Distance m
4	1	79.32	90	--	1.58
4	2	81.54	90	--	1.99
4	3	84.57	90	--	3.10
4	4	77.82	90	--	1.39
2	9	93.3	69	17.7	0.905
2	10	96.3	69	14.7	1.08
2	11	98.8	69	12.2	1.29
2	12	102.25	69	8.75	1.78
5	13	77.58	90	--	1.36
2	14	101.0	69	10.0	1.57
5	14	79.25	90	--	1.57
5	15	76.22	90	--	1.23

Notes:

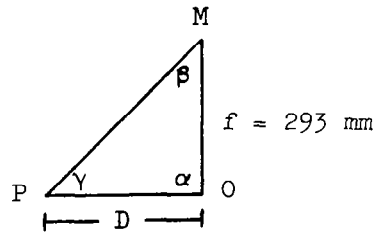

For $\beta = 90°$, $D = f/\cos \alpha = \frac{0.293}{\cos \alpha}$ (Meters)

For $\beta = 69°$, $D = f \frac{\text{Sin } \beta}{\text{Sin } \gamma} = \frac{0.2735}{\sin \gamma}$ (Meters)

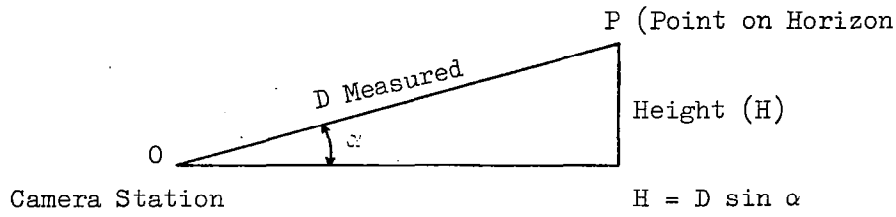

The height of the crater rim above the camera station is 9.4 meters for the right view and 4.72 meters for the left view.

This difference in elevation may be due to actual variation in the crater horizon, or may be caused by difference in the slope of the surface on which the distances were measured. In either event, the left and right view distances are computed separately.

Vertical angle measurements were made between the true and image horizon at 10° intervals around the panorama, except where the horizon was obviously obscured. The distances of the true horizon from the camera station were computed, as summarized in Table 5.

The general shape of the crater was determined by plotting the azimuth and distance found for the several points, as shown in Figure 21. The disparity in the left and right view distances are apparent attempts to fit a curve to the plotted points.

The right-hand set of points fit a circle of 118 meters radius, the center of which is 52 meters from the camera station, at an azimuth of 205°. The

TABLE 5. HORIZON DISTANCE CALCULATIONS

	Azimuth	Elevation angle (α) Measured	Height Calculated ($H = D \times \sin \alpha$)	Distance Calculated ($D = H/\sin \alpha$)
	(°)	(°)	m	m
Left View	240	1.57	4.72	172
	250	179.0	4.72	151
	290	3.63	4.72	75
	300	4.04	4.72	67
	306	4.1	4.72	66*
Right View	57	7.72	9.4	70*
	60	7.72	9.4	70
	70	7.41	9.4	73
	80	7.10	9.4	76
	90	6.33	9.4	85
	100	5.87	9.4	92
	110	5.40	9.4	100
	140	4.17	9.4	129

*Measured values from mirror images.

left-hand set fit a circle of 164 meters radius, the center of which is 103 meters from the camera station, at an azimuth of 171°.

By fitting both sets of points to a curve analytically and/or graphically, the curve takes the shape of an ellipse. The ellipse is shown in Figure 22, and has a major axial distance of 286 m; a minor axial distance of 216 m; and an eccentricity of .755. The center of the ellipse is 81 m from the camera station at an azimuth of 200°.

The true shape of the crater may correspond to the ellipse as described. However, the ellipse may be the result of the accumulated errors in the distance determination, tilt calculation, tilt azimuth, empirical analysis, etc.. Whether the crater shape is elliptical or circular, the radial dimensions will be in the order of the radii as determined above, i.e., between 108 and 164 meters. Since an elliptical shape fits the empirical data in hand, this will be assumed as the true shape of the crater. Relative errors will be small.

To find the true azimuth and distances for points in the panorama, the procedure is outlined below:

True Azimuth

(1) Construct the true horizon curve. This may be done using the formula in Section 3.1, or the values in Table 6.

(2) Drop perpendicular to the true horizon from the image point.

TABLE 6. IMAGE DISTANCE OF TRUE HORIZON ABOVE OR BELOW CENTERLINE

Quadrant	Quadrant	Quadrant	Quadrant	Distance Values
I	II	III	IV	
+(°)	+(°)	-(°)	-(°)	mm
0	360	180	180	112.5
5	355	185	175	112.2
10	350	190	170	110.8
15	345	195	165	108.8
20	340	200	160	105.8
25	335	205	155	102.1
30	330	210	150	97.4
35	325	215	145	92.2
40	320	220	140	86.3
45	315	225	135	79.6
50	310	230	130	72.4
55	305	235	125	64.6
60	300	240	120	56.3
65	295	245	115	47.6
70	290	250	110	38.5
75	285	255	105	29.4
80	280	260	100	19.6
85	275	265	95	9.8
90	270	270	90	0.0

Notes:

$$Y = r \tan \theta \cos \alpha$$

$$= (293 \text{ mm}) (\tan 21°) \cos \alpha$$

$$= (293 \text{ mm}) (0.3839) \cos \alpha$$

$$= 112.5 \text{ mm} \times \cos \alpha$$

(3) Read the true azimuth at A, the intersection of the perpendicular and the true horizon, as shown below:

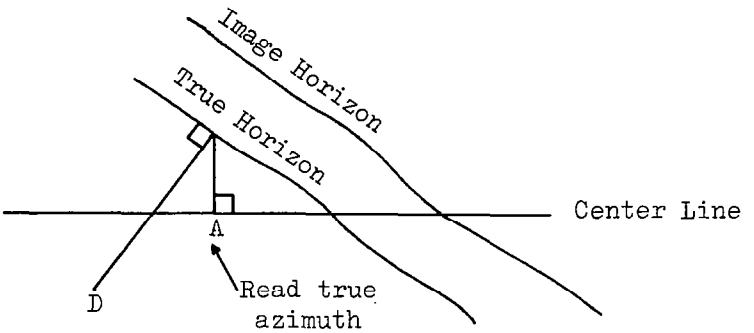

Distance

The following formulas are the relationships between the slope of the ground (φ), the angle of inclination (θ), and the line-of-sight distance (D).

The slope of the ground (φ) may be computed from a known distance point; θ is the angle between the point and the constructed horizontal curve.

The pertinent formulas are:

$$(1) \quad \varphi = \tan^{-1}\left[\frac{.56 \pm D \sin \theta}{D \cos \theta}\right]$$

The negative sign is used for points below the true horizontal, and the positive sign for points above the true horizontal.

$$(2)\quad \theta = \sin^{-1}\left(\frac{.56}{D}\cos\varphi\right) - \varphi$$

The angle of inclination (G) is usually measured directly on the imagery.

$$(3)\quad D = \frac{.56\cos\varphi}{\sin(\varphi \pm \theta)}$$

The sign is negative above the true horizontal, and positive below.

These formulas were used to construct the overlays for the third panorama. They are generally true, except in the central portion of the panorama, where local irregularities prevent systematic grid construction.

3.2 MIRROR IMAGES

There are three pairs of dihedral mirrors present in the Luna 9 panoramas. The purpose of the mirrors is to provide some means of making measurements with a single camera.

3.2.1 GENERAL CONSIDERATION. Figure 23 is a sketch showing the geometric relations of a dihedral mirror, the dihedral angle being that formed by the intersection of the two reflecting surfaces.

Some of the pertinent relationships are:

(1) The angle of incidence (i) = angle of reflection (r).

(2) The dihedral angle between the mirror is $r_A + r_B$, i.e., the sum of the reflecting angles of the two mirrors. If the mirrors are perpendicular (right angle mirrors), the dihedral angle is 90°; r is 45°; and $r_A = r_B = i_A = i_B$.

(3) The central reflecting angle = 180° - 2r; in the case of a right dihedral mirror, $\beta = 90°$.

(4) For a point at infinity (P'), the line-of-sight OP' is parallel to the reflected ray MP; and the azimuth angle of the point is = 180° - β = 2r.

(5) The plane determined by the point; its mirror image; and the panorama center, intersects the panorama in a line parallel to the center line of the panorama. The image of the point; and the mirror image, will be at an equal distance above or below the center line.

(6) If the mirror dihedral angle is a right angle; and if mounted symmetrically to the optical center, the azimuth angle (α) will be 90° or less for all images. Points on the horizon will be 90° from the mirror.

(7) Knowing angles α and β, and the distance f (radius of the panorama), distance d may be calculated using the law of sines and the law of cosines:

Law of Cosines $t^2 = d^2 + f^2 - 2df \cos \alpha$

Law of Sines $\frac{\sin \alpha}{t} = \frac{\sin \beta}{d} = \frac{\sin \gamma}{f}$

For images above or below the center line, f will become larger. This correction causes a maximum of 4% error in f, however, this error may be neglected for present purposes.

3.2.2 LUNA 9 MIRROR IMAGES. The first mirror image found on the panorama was that of mirror 3 at a latitude of -4° and immediately to the left of the first dihedral mirror at 315°. This leads to one of two conclusions: (1) either the mirrors of the second dihedral pair are not at right angles, i.e., not reflecting at 90°; or (2) the dihedral pairs are not displaced at exactly 90°.

By projecting the mirror image to the horizon, it is noted that the intersection is approximately 90°. Consequently, the conclusion is that the second pair of mirrors are right dihedral mirrors; but the displacement angle between the first and second mirror pairs is less than 90°.

The horizon reflected in mirror 4 is found at a point 90° to the right of the mirror (azimuth 120°) between two large craters. This confirms the second dihedral mirror as a right angle pair placed in a symmetrical position with respect to the optical center of the scan.

The reflected image for mirror 5 was found at an angular distance of slightly less than 80°, crossing a small craterlet at 55°, +4°. Again,

the projection of the mirror image will intersect the horizon at nearly 90°. Its complementary mirror (no. 6) reflects only the lunar sky, except for a small unidentified portion of the spacecraft at its lowest most edge. This dihedral pair, because of its image width; intersection with horizon; and marked symmetry (as seen in the panorama) is assumed to be a right dihedral, symmetrically oriented, mirror pair.

In attempts to locate the mirror image of the first dihedral pair (mirrors 1 and 2), it became apparent that its orientation was somewhat different than the other two.

The boulder on the horizon as reflected in mirror 1 cannot be found on the horizon as shown in the same panorama. However, the image is found on the first panorama where the horizon is not obscured by the latch mechanism at 250°, -10°. The mirror image is about 62° to the left of the mirror.

Attempts to find the image of mirror no. 2 to the right of the second dihedral pair (since the angle between the first two pairs is less than 90°) led to the discovery of a common point with mirror no. 5. This common point is at the crater at 54°, +4° mentioned above. The intersection of the projected mirror image with the horizon is about 110° to the right of the mirror.

Since the scans of the azimuths of mirror images at the horizon for mirrors 1 and 2 is 160°, or approximately 180°, it may be assumed that this is a right dihedral mirror, set as an asymmetric orientation with respect to

the optics center. Calculations confirm the configuration as shown in Figure 24. The asymmetric positions may have been intentional, or accidental, due to malfunction or damage on impact.

3.2.3 MIRROR IMAGE DISTANCE CALCULATIONS. Table 4 summarizes the distances calculated from the angular measurements made from the mirror images. The true reflection angle of mirror 2 is found by using point no. 14 whose distance was determined from mirror 5.

In calculating the mirror images distances, the focal distance, or radii to the mirrors is of prime importance. It is assumed that the maximum distance was used, i.e., the mirrors were placed at the extreme edge of the capsule to give the longest base possible for distance computation.

The limitations for distances measured are: four times the base distance, and 20 times base distance. These limits, in the Luna 9 images are 1.2 meters and 6 meters, using a maximum base of 30 cm. At points closer than this, the stereoscopy (or identification of the same point from two different views) becomes difficult or impossible. For more distant points the errors due to small angular differencies become too great for accurate calculations. It may be concluded that the Luna 9 arrangement was made for measurement of near objects on the lunar surface, and to give a scale factor for a limited number of points in the near field of view.

3.3 STEREOSCOPIC PANORAMAS

The increase in tilt of the camera system, between scanning times of the first and third panoramas, lends itself to possible stereoscopy, and three-dimensional viewing of the lunar scene. The areas where this may be possible are seen in Table 2 where the panoramas overlap. These are: (1) from 238° to 298° in Frames A and B, and (2) from 60° to 144° in Frames F and G.

The vehicle supposedly tilted by rotating about the point of contact with the surface. Figure 25 shows the amount of displacement of the camera center as a result of the tilt. The diagram presents the camera system in cross-section, perpendicular to the axis of tilt. The maximum distance between centers in this plane is 8.4 centimeters (about 3.4 inches), or slightly larger than the normal eye base.

The most satisfactory stereoscopy is obtained by placing the panoramas under a stereoscope and orienting by rotating each about the intersection of the center line and the 90° (or 270°) marks on the panorama. The horizon on the two panoramas should be parallel to the eye base (or stereoscope base) for best depth perception.

The stereoscopic view thus obtained is a distorted model, due to the cylindrical nature of the image plane. When the circular image plane is placed flat for viewing, the features are displaced from their true position, giving a false parallax. It was, therefore, necessary to rectify the imagery in order to permit accurate viewing and measuring in a conventional stereoscopic plotter.

The photography was rectified by mounting the panorama on a section of a cylindrical surface with a radius of curvature equal to the effective focal length. The panorama was oriented with the optical axis of the copy camera perpendicular to the point of true horizon on the panorama (i.e., the intersection of the center line and the 90° mark on the true horizon curve). The rectified photograph was, in effect, a standard perspective view taken with the camera axis horizontal. Figure 26 is a print of a rectified image.

The photo base of the imagery, so prepared, was 6.5 mm. Using the standard formula,

$$Y = \frac{bf}{p}$$

Y = horizontal distance

b = base distance

f = focal distance

p = parallax base

with the base distance value of 8.4 cm and a focal length of 300 mm, the effective horizontal distance Y was computed as 3.88 meters. The plotting scale (at no enlargement) is p/b (or $\frac{f}{Y}$) = 1:13. A differential parallax of 0.5 mm gives a differential horizontal distance of $\frac{1}{4}$ meter.

These values were used in plotting vertical profiles from a stereoscopic pair of rectified frame F and F_3 panoramas. An enlargement of the results is shown in Figure 27. A topographic map may be prepared from these

profiles using the similar (plotting scale values) techniques.

A more direct method of preparing topographic maps from the rectified imagery is to use a terrestrial plotter, or a universal plotter in which the Y-Z axis may be interchanged.

3.4 PARTICLE SIZE DISTRIBUTION

The lunar surface as seen in the Luna 9 imagery is not homogeneous. This may be seen by a casual inspection of the imagery. The low resolution of the imagery and presence of shadows inhibit the recognition of discrete rock particles, especially as the distance from the camera increases. Any general action concerning particle size distribution is, thus, subject to numerous errors.

A particle size count was made in Frame F_3, which offered the best continuous unobscured view to the horizon. The results of the count and particle size determinations are shown in Table 7. The 60 small particles (3.5 to 8.0 mm diameter) were counted in random sample areas of distances 1.6 to 4.0 meters from the spacecraft, where views were least obscured. The remaining or 61 coarse particles (8 to 158 mm diameter) were counted in an area of distances of 1.8 to 8.6 meters from the spacecraft. In an area between the horizon and 8.6 meters from the spacecraft, 9 particles were recognizable, but were so obscure that size determination was impossible.

A cumulative curve of coarse rock particles is shown in Figure 28. The curve resembles a standard cumulative curve except at point A and B. At

TABLE 7. PARTICLE SIZE COUNT AND CLASSIFICATION (FRAME F_3)

Particle Size	Number of Particles	Cumulative Number	Area of Count	Number of Particles	Wentworth Size Classification
mm		>8mm	(m^2)	per $10m^2$	
3.5					Granules
4					
5	60		0.75	80	
6					
7					
8	2	2	5.38	2^3	
9	2	4	5.38		
12	1	5	18.68		
13	1	6	18.68	12.9	
14	1	7	18.68		
16	1	8	18.68	2^4	
18	3	11	18.68		
20	3	14	18.68		
21	4	18	18.68		
23	2	20	18.68		
25	2	22	18.68	14.5	Pebbles
26	2	24	18.68		
27	1	25	18.68		
28	2	27	18.68		
29	3	30	18.68		
30	1	31	18.68		
31	3	34	18.68		
32	1	35	18.68	2^5	
33	1	36	18.68		
35	1	37	18.68		
36	1	38	18.68		
37	3	41	18.68		
38	1	42	18.68		
39	3	45	18.68		
40	2	47	18.68	11.2	
41	1	48	18.68		
42	1	49	18.68		
47	1	50	18.68		
48	1	51	18.68		
51	2	53	18.68		
52	1	54	18.68		
53	1	55	18.68	2^6	
					Cobbles

Table 7.
(cont'd)

Particle Size	Number of Particles	Cumulative Number	Area of Count	Number of Particles	Wentworth Size Classification
mm		>8mm	(m^2)	per $10m^2$	
69	1	56	18.68		
78	1	57	18.68		
82	1	58	18.68	2.1	Cobbles
109	1	59	18.68		
128	1	60	18.68	2^7	
158	1	61	18.68	1.6	
256	0	61	18.68	2^8	
					Boulders

point A, the curve shows sharp deviation, probably due to the rapid deterioration of resolution in the smaller particle size range. At point B, the curve has a marked shift toward the coarse fractions. This may be due to a similar limit of resolution in the more distance portions of the view. The same effect would be caused by an admixture of materials from two different sources. This, again, is suggestive of the coarser particles being fragments of the spacecraft littering the scene.

A particle size distribution curve is shown in Figure 29. The extrapolation of this curve to particle sizes other than those actually counted, or generalizations made on areas outside the 19 square meter sampling area, should be made with extreme caution.

3.5 CRATER SIZE DISTRIBUTION

Identification of craters on the Luna 9 panoramas is more difficult than identification of particles. The crater itself is easily obscured by the surface when viewed from an angle. This is true on relatively flat surfaces, as opposed to the distinct positive relief exhibited by a rock particle.

A count was made of the craters that could be positively identified on the third panorama. The count of the small craters was limited by the inability to draw a distinct boundary between craterlets and small irregularities or vesicular pores. Near the horizon, only the larger craters could be counted because of poor resolution of the photography and masking by the angle of view and surface irregularities of other craters.

The counts were made in accordance to surface area, as follows: (1) from the nearest foreground (about $\frac{1}{2}$ meter) to a distance of 2 meters; (2) from an area of 2 to 5 meters; and (3) from an area of 5 to 30 meters. At distances greater than 30 meters, craters were either not identifiable, or were so obscure that no reliable measurements could be made.

A total of 44 craters were counted, the greater number falling in the nearest area. These results are presented in Figure 30 in the form of simple histograms. The histograms show a different maximum for each of the three areas. Two (A and C) show a skewed curve, and one (A) shows a secondary maximum for the larger size craters. The cumulative curve shows the several maxima, the largest being between 2^6 to 2^7 (64 to 128) mm. The maxima seems to be cylical, occuring in every other step. The recurring peaks may be due to size, but may also be due to the decrease in resolution with distance. The latter is the most likely explanation.

A crater size distribution graph is shown in Figure 31. The plotted points deviate from the linear graph at both the lower and upper ends. The deviation in the smaller sizes is due to the difficulty of distinction between craters and surface irregularities or vesicles. The deviation in the larger sizes is due to the limited area covered by the imagery. It may be of interest to note that the total area of the small (32 to 128 mm diameter) craters accounted for 7% of the total surface area; the intermediate size (128 to 1024 mm diameter) crater area was 24% of the total area; while the large size (1.024 meters and above diameter) crater area gave a figure of 18%.

It is somewhat dangerous to extrapolate these figures to areas outside the immediate vicinity of the Luna 9 spacecraft. This should be obvious when it is realized that the statistical count was made of an area of less than 1/10 of a hectare, or $\frac{1}{4}$ of an acre.

SECTION 4

SUMMARY AND CONCLUSIONS

The Russian Luna 9 space vehicle contained a simple panoramic camera mechanism. The camera system provided telemetered photographic panoramas of the lunar landscape.

Simple measurements and calculations reveal that the spacecraft made a soft-landing near the edge of a crater with a maximum diameter of 330 meters and a minimum diameter of 210 meters. The camera system is 4 to 9 meters below the rim of the crater.

The surface materials consist of a highly vesicular to frothy bedrock with scattered particles up to cobble size. The loose particles are unevenly distributed over the surface. Craters, both rimmed and without rims, are visible throughout the area and range in size from 15 meters in diameter to those barely visible. The spacecraft itself is located on the rim of a small crater of 4.8 meters diameter.

The field of view from the spacecraft center is highly confined by the rim of the crater; and as a consequence, results of both qualitative and quantitative investigations should be recognized as limited to a specific local environment.

APPENDIX

ILLUSTRATIONS

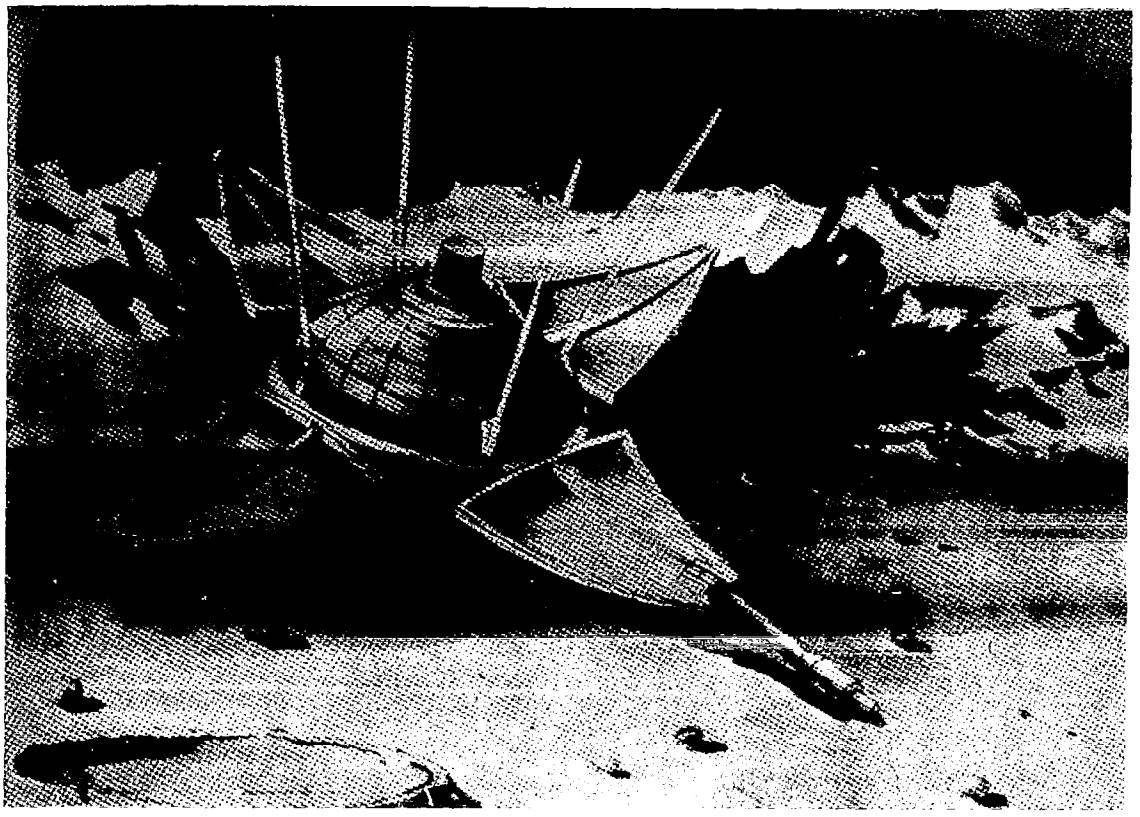

FIGURE 1. SOVIET SKETCH OF LUNA 9 CAPSULE

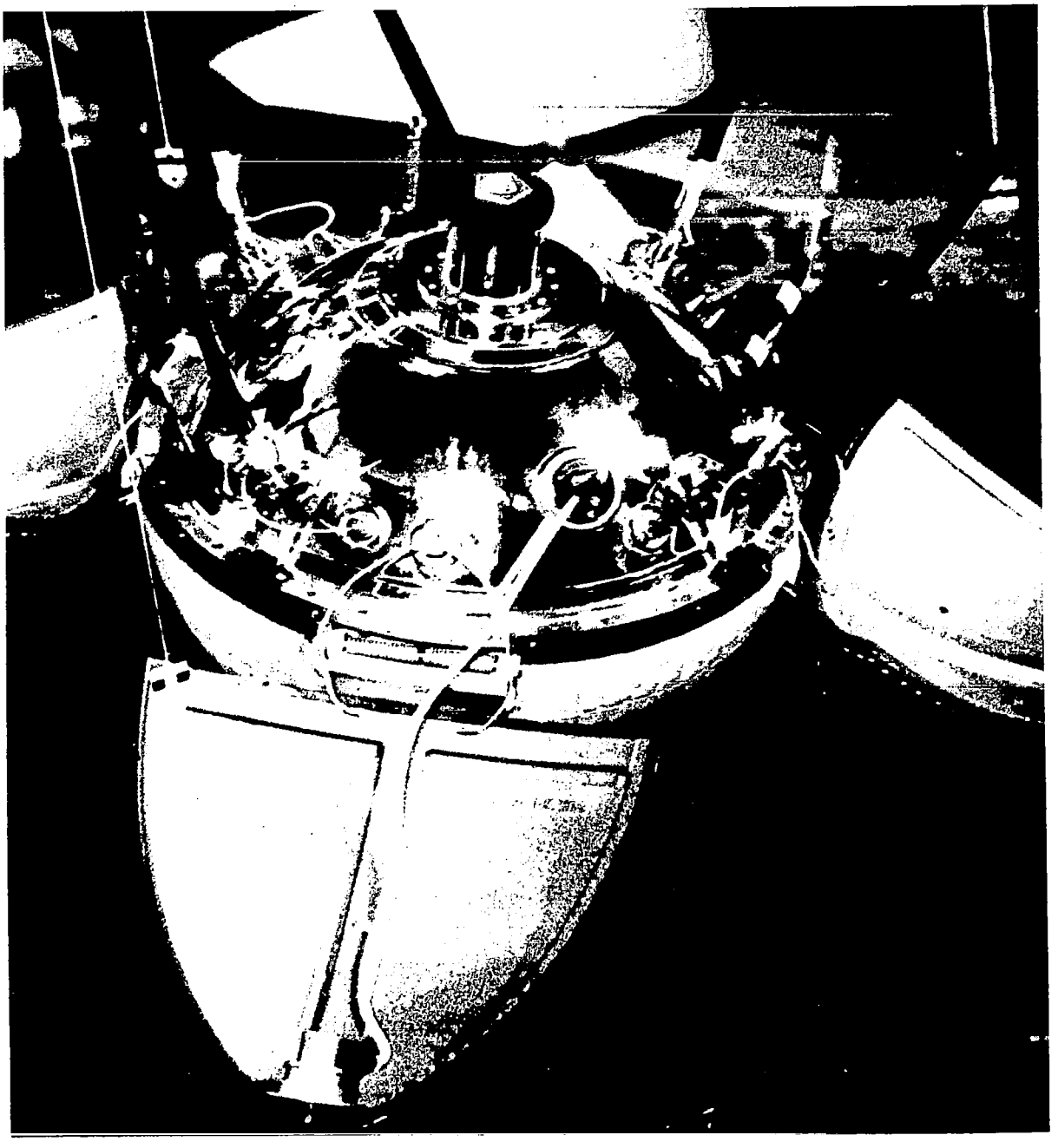

AVIATION WEEK AND SPACE TECHNOLOGY

FIGURE 2. PHOTOGRAPH OF LUNA 9 CAPSULE

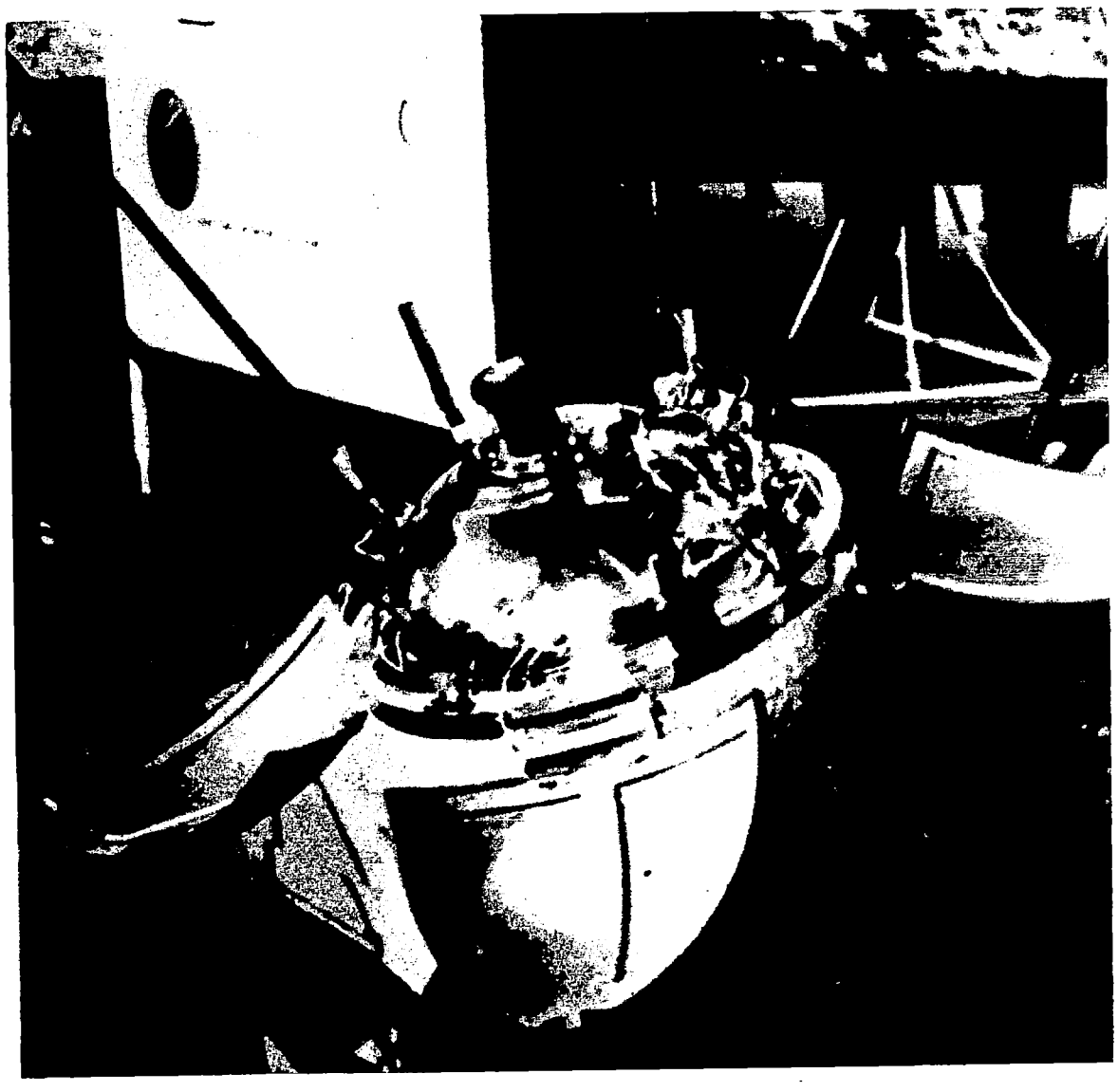

AVIATION WEEK AND SPACE TECHNOLOGY

FIGURE 3. PHOTOGRAPH OF LUNA 9 CAPSULE

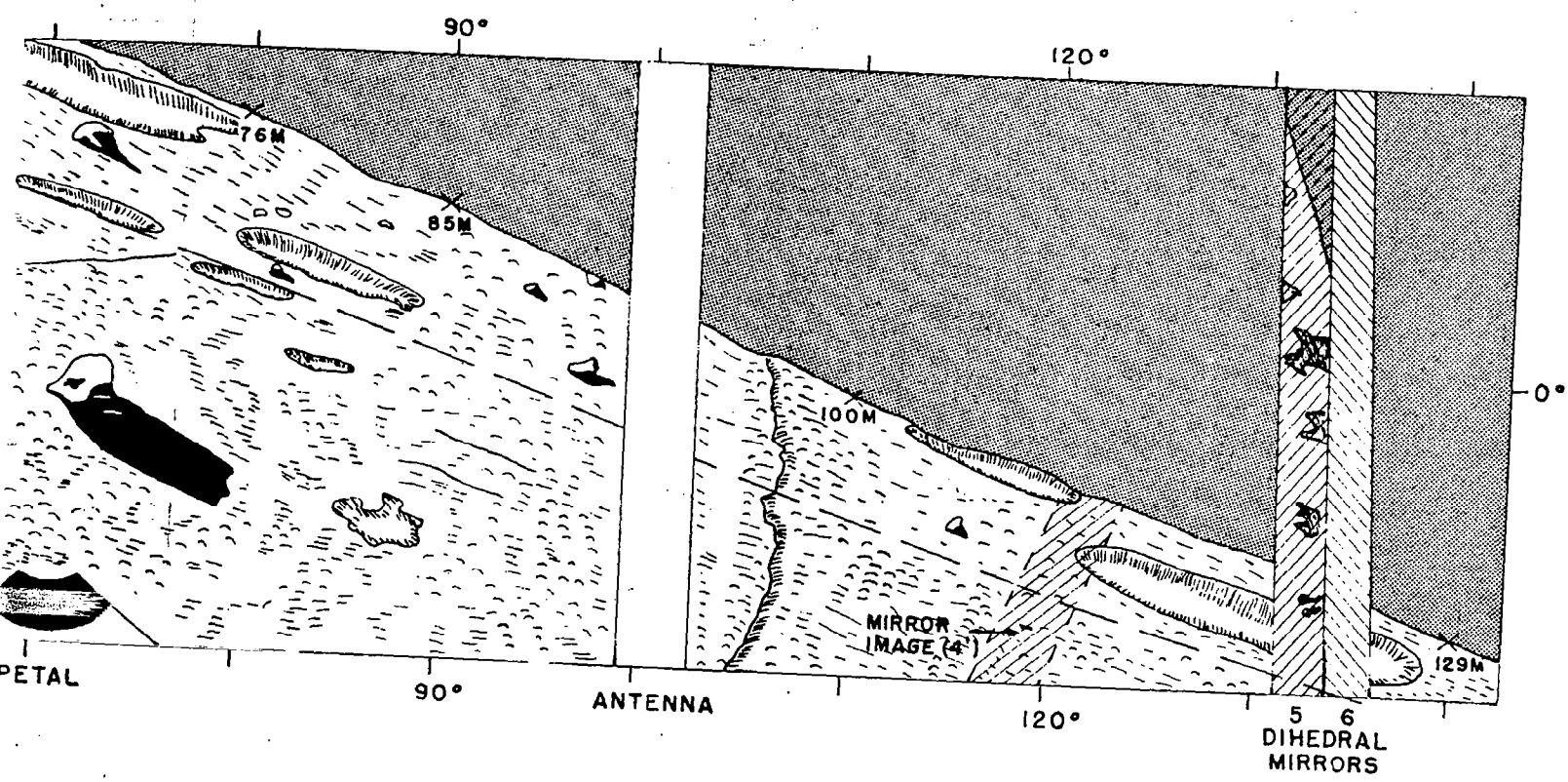
90°
120°
76M
85M
100M
0°
MIRROR
IMAGE (4')
129M
PETAL
90°
ANTENNA
120°
5 6
DIHEDRAL
MIRRORS

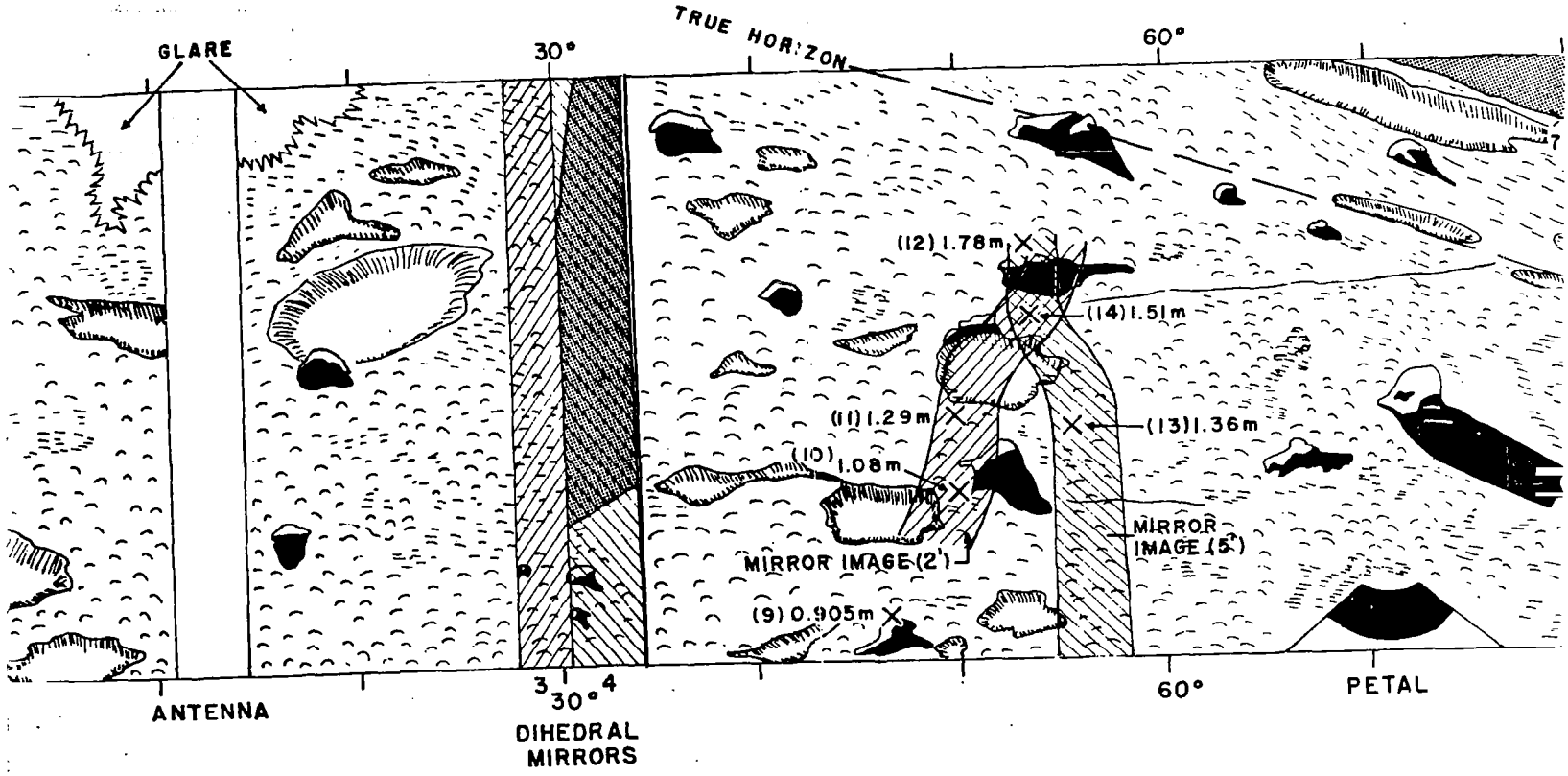

RAMA TAKEN FEBRUARY 5, 1966 (TILT 21°; SUN ELEVATION 27°)

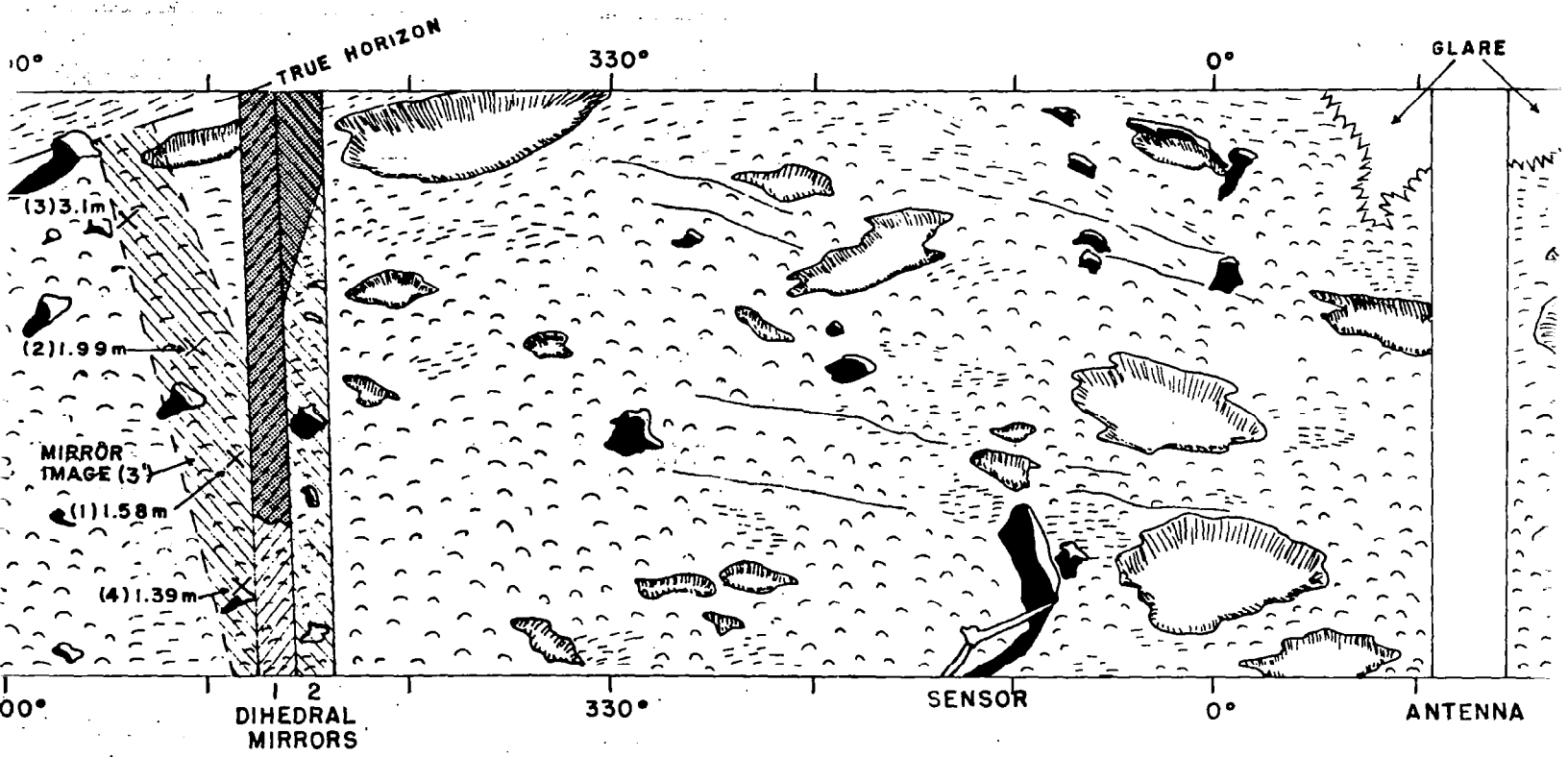

FIGURE 4. SKETCH OF PORTION OF LUNA IX PANORAMA TAKEN FR

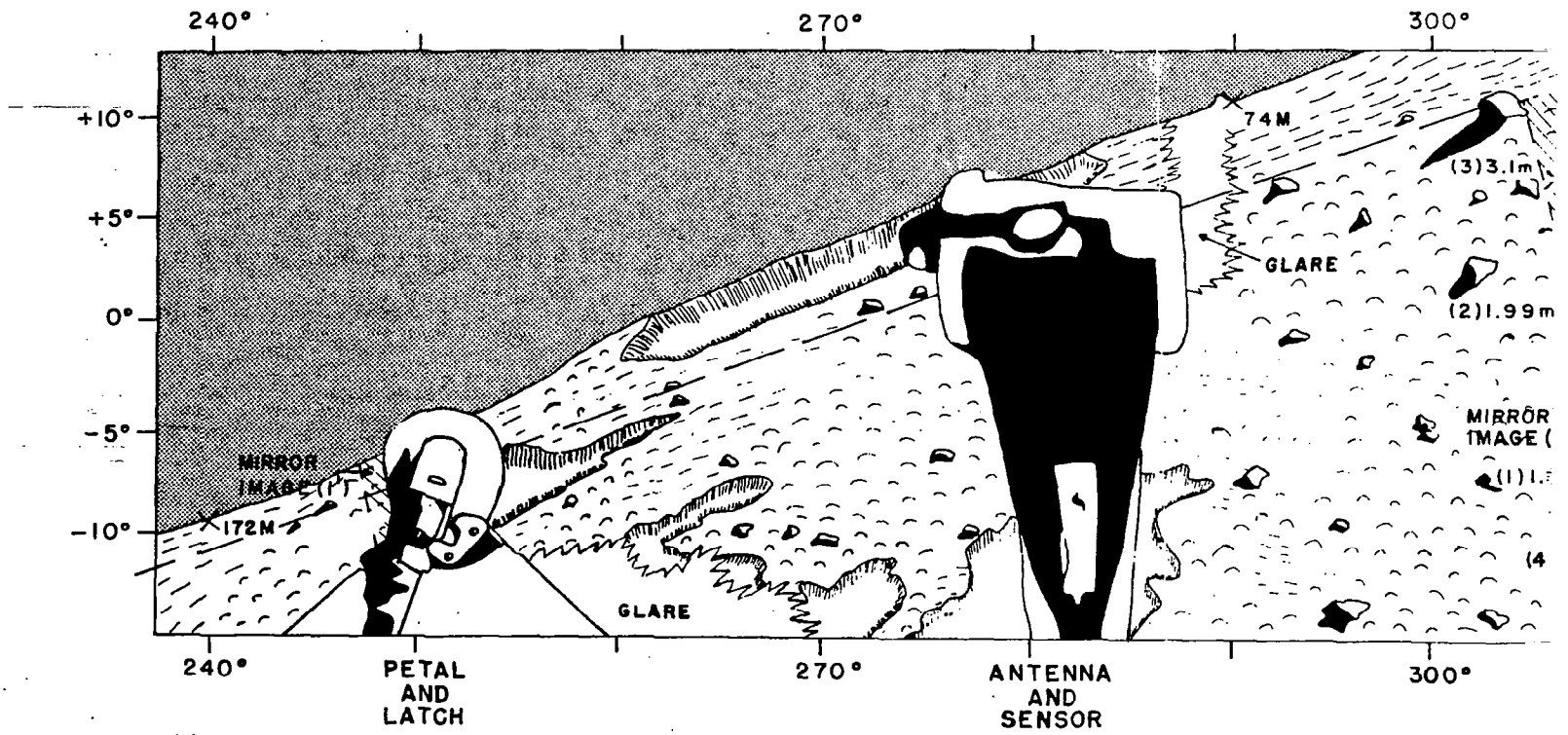
240°
270°
300°
+10°
+5°
0°
-5°
-10°
74M
(3)3.1m
GLARE
(2)1.99m
MIRROR
IMAGE (
(1)1.
(4
MIRROR
IMAGE (1)
172M
GLARE
240°
PETAL
AND
LATCH
270°
ANTENNA
AND
SENSOR
300°

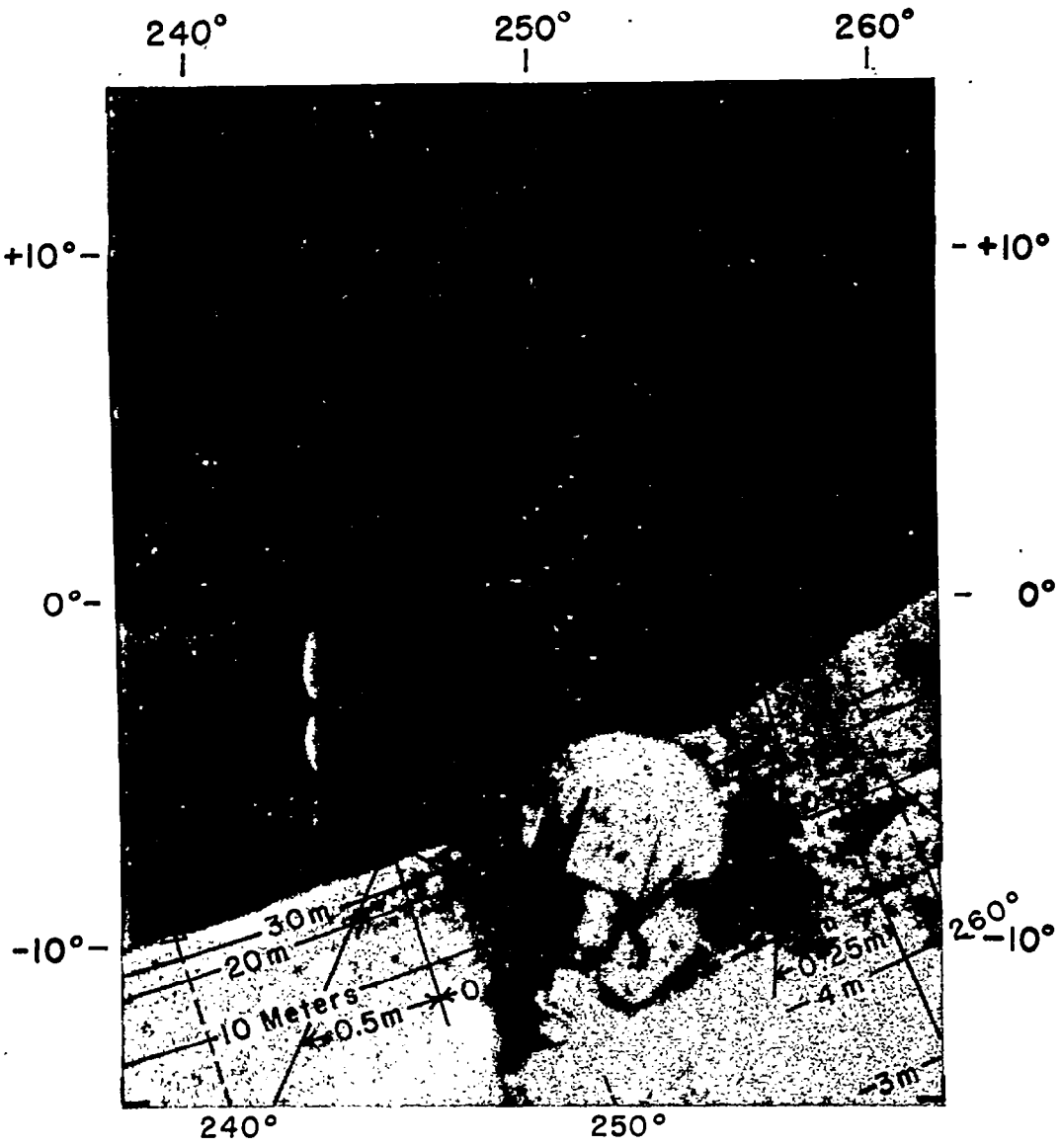

FIGURE 5. FRAME A_3

FIGURE 6. FRAME B_3

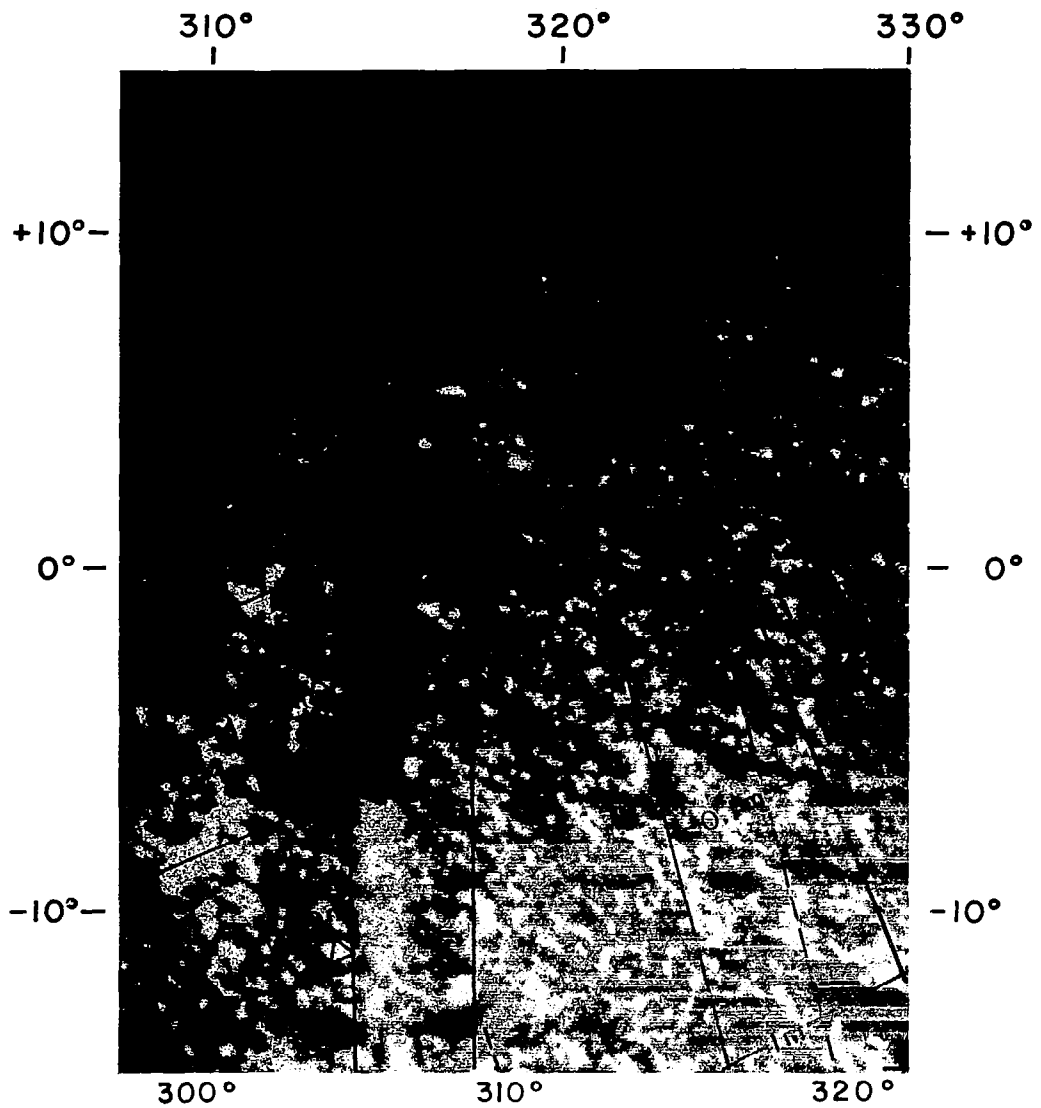

FIGURE 7. FRAME C_3

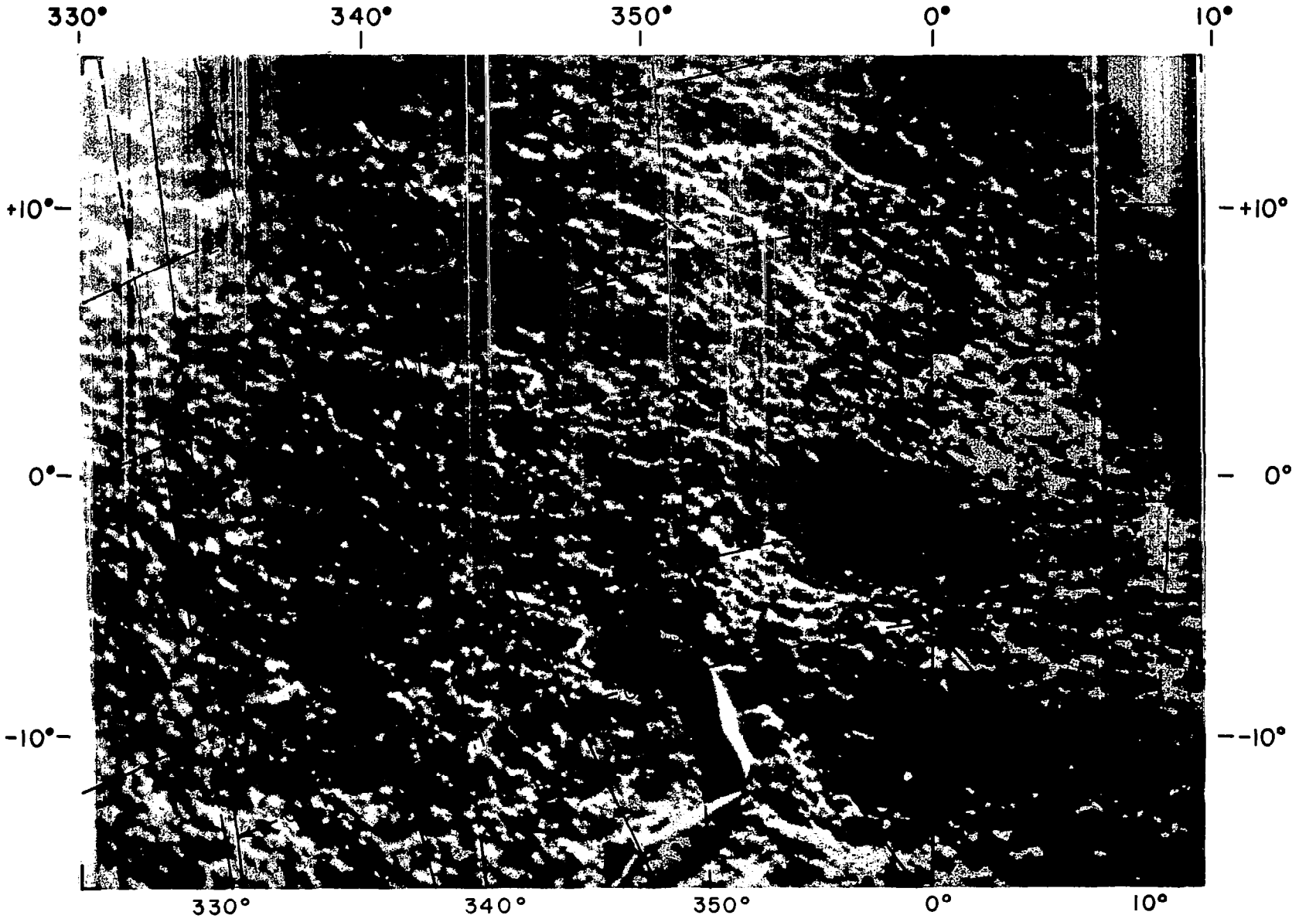

FIGURE 8. FRAME D_3

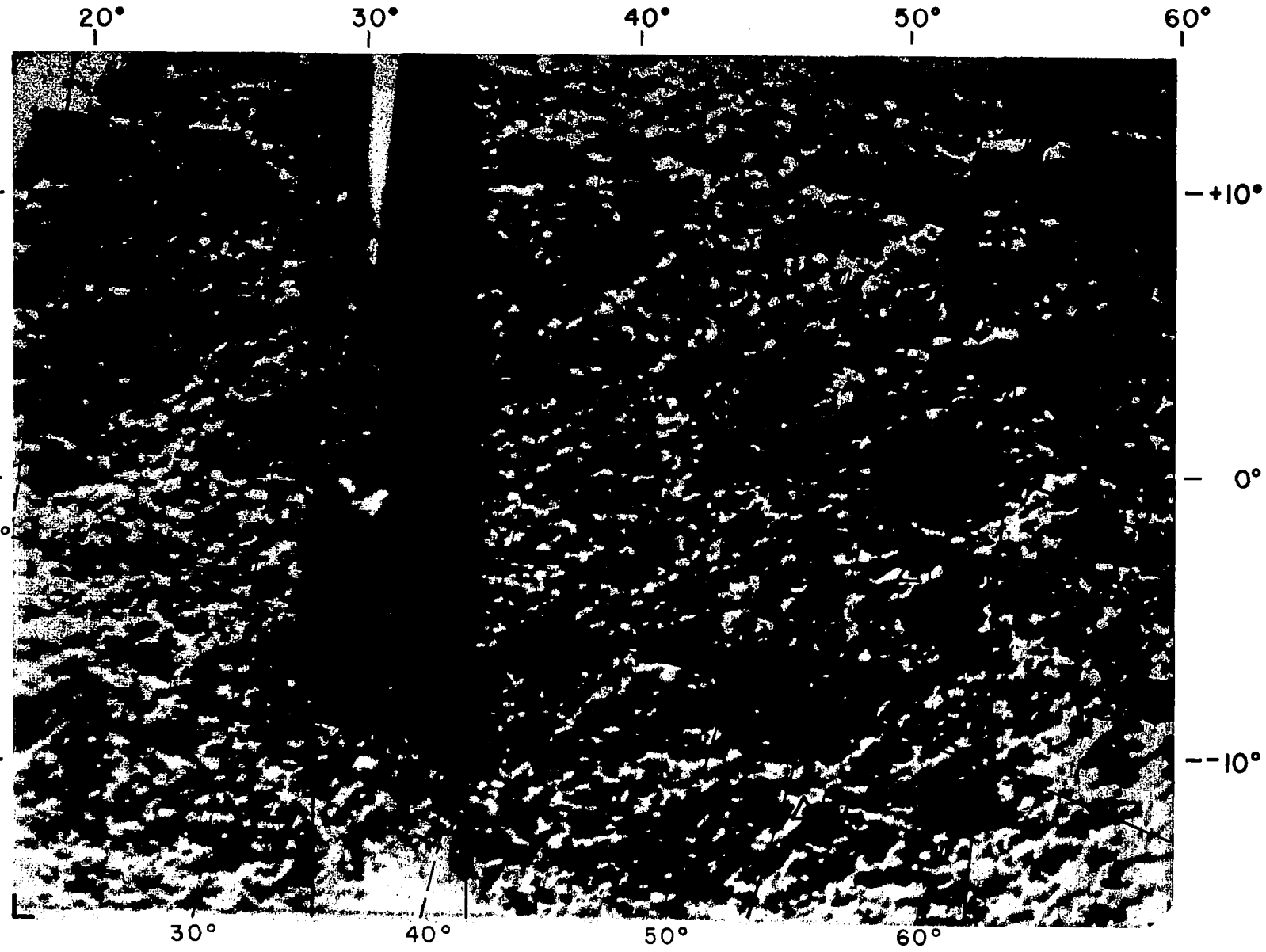

FIGURE 9. FRAME E_3

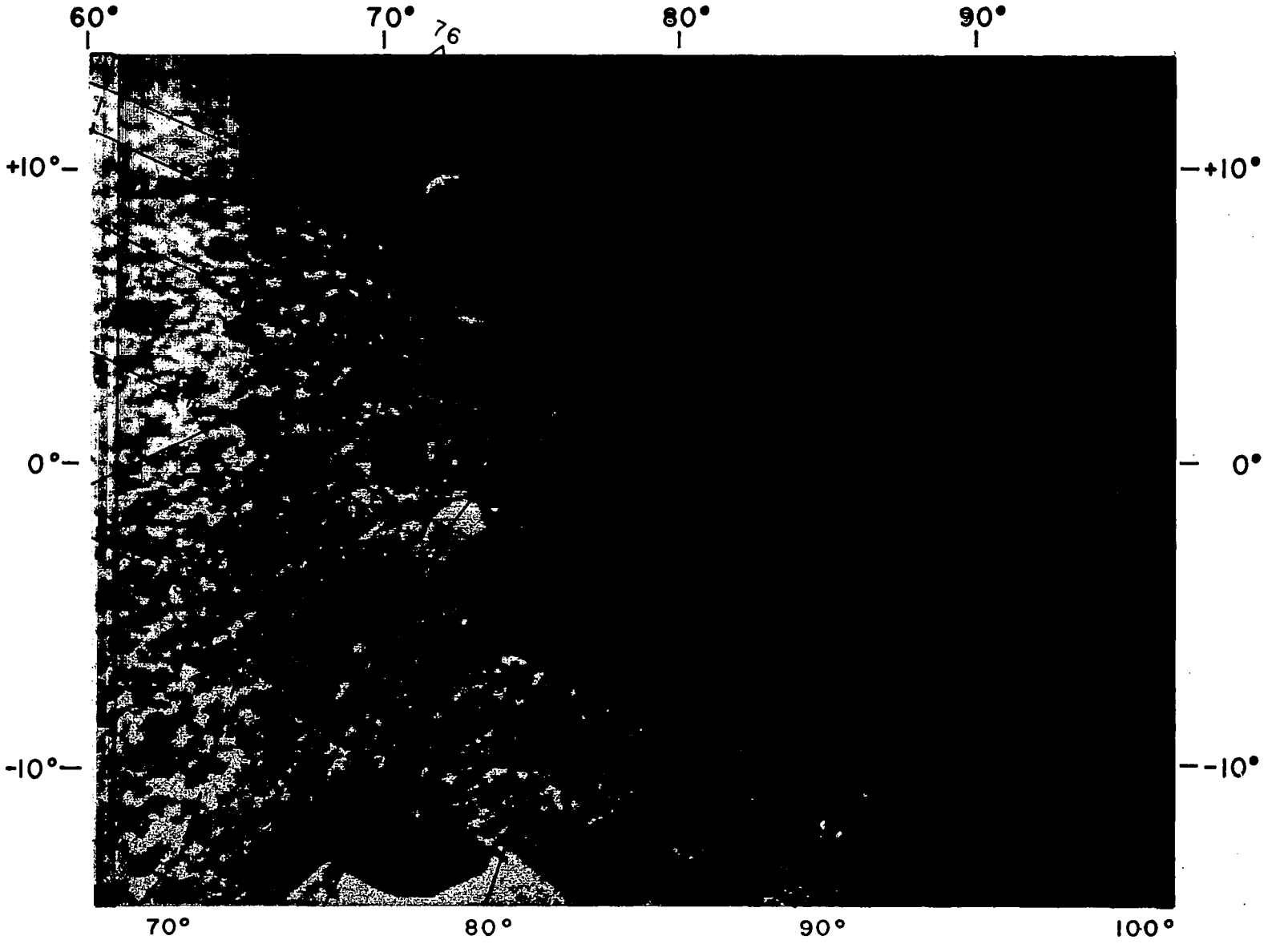

FIGURE 10. FRAME F_3

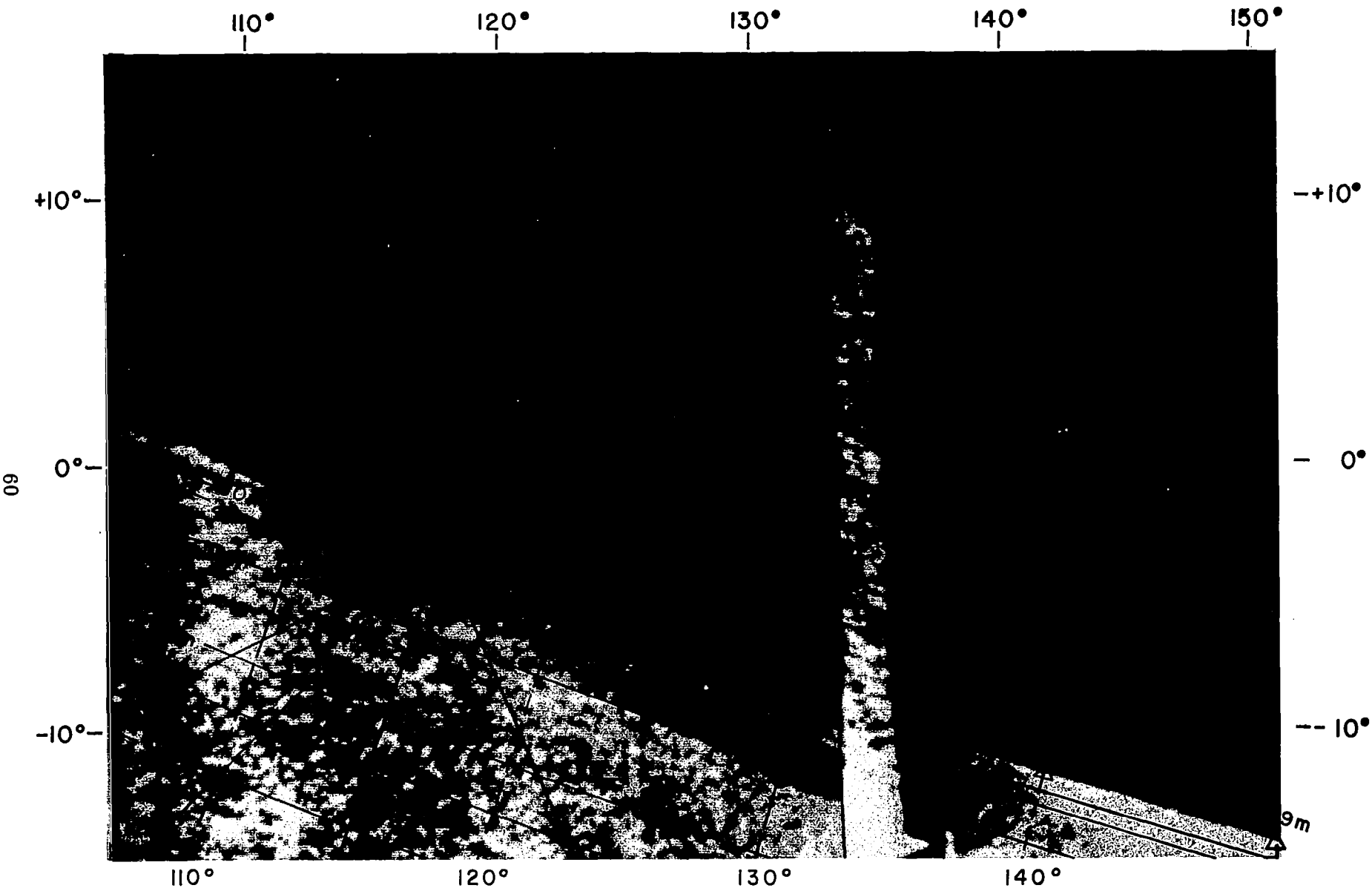

FIGURE 11. FRAME G_3

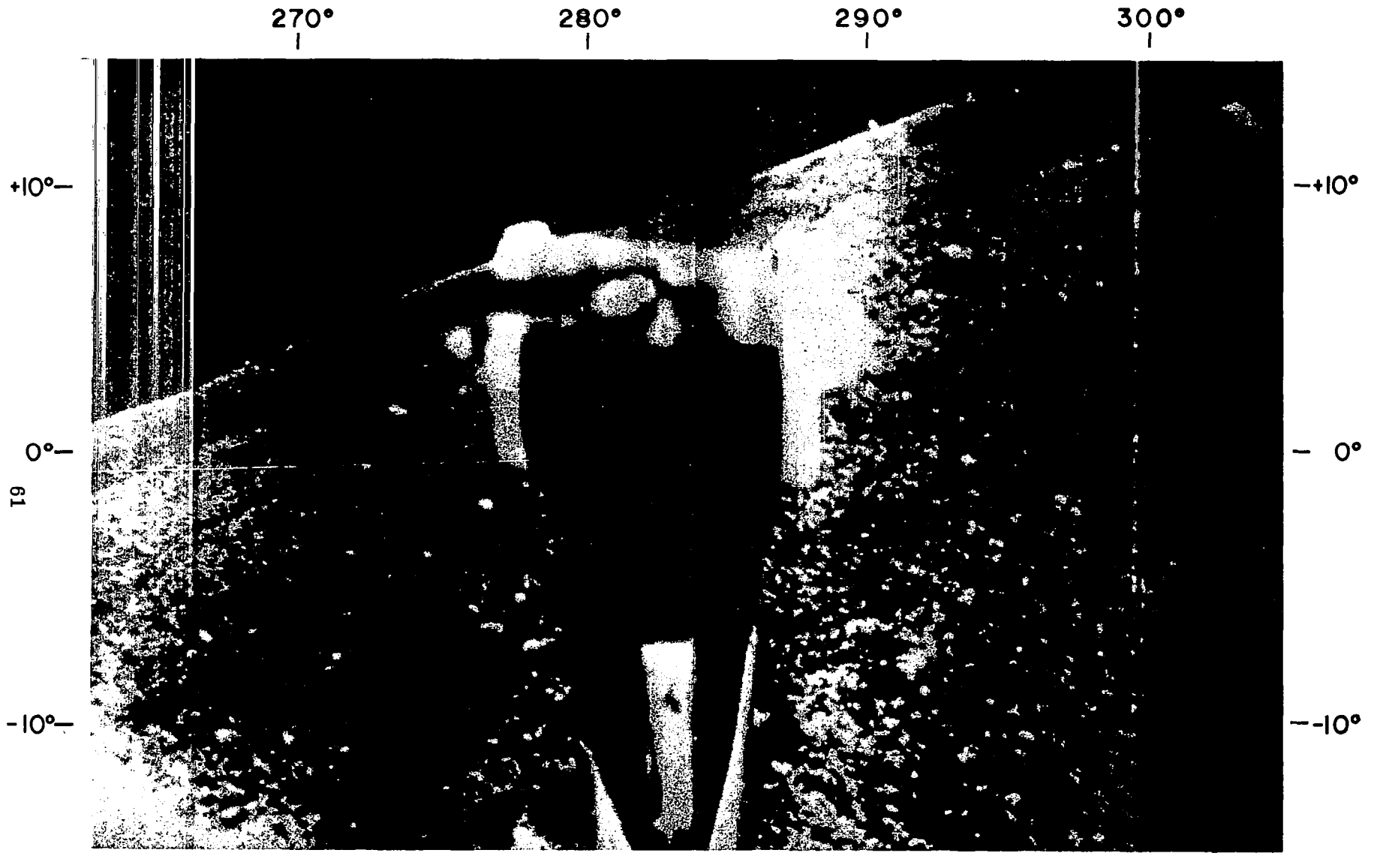

FIGURE 12. FRAME B_2

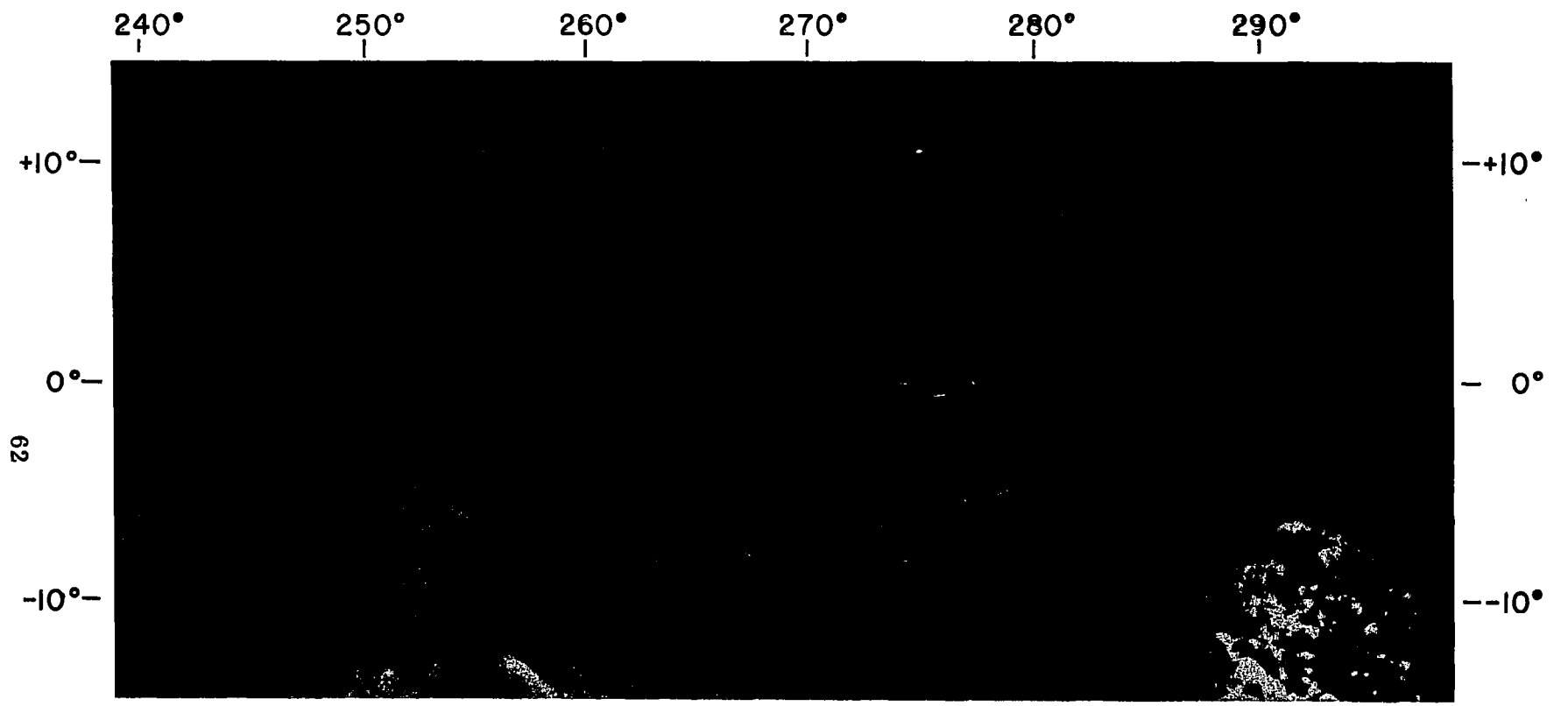

FIGURE 13. FRAME A,B,

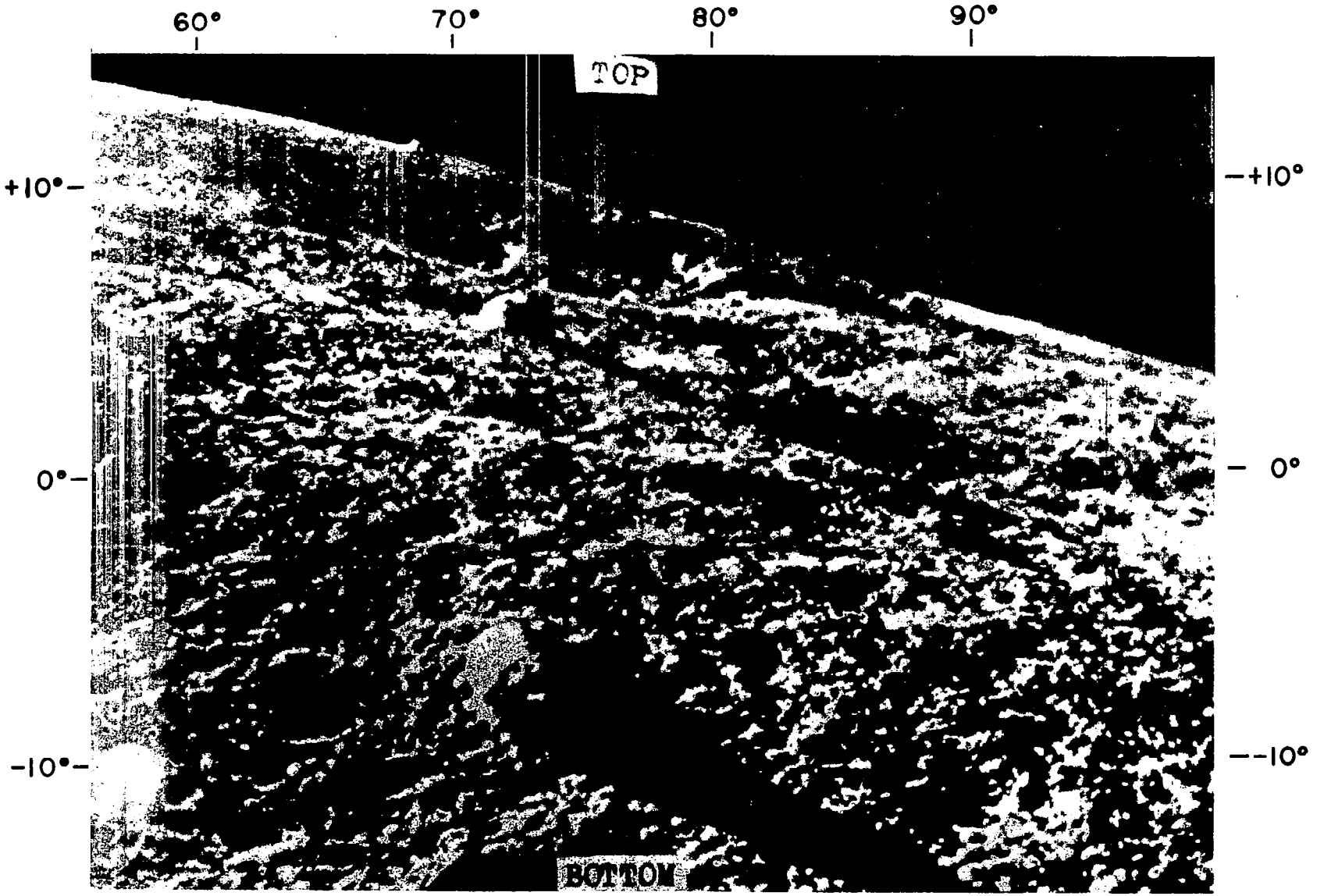

FIGURE 14. FRAME F_1

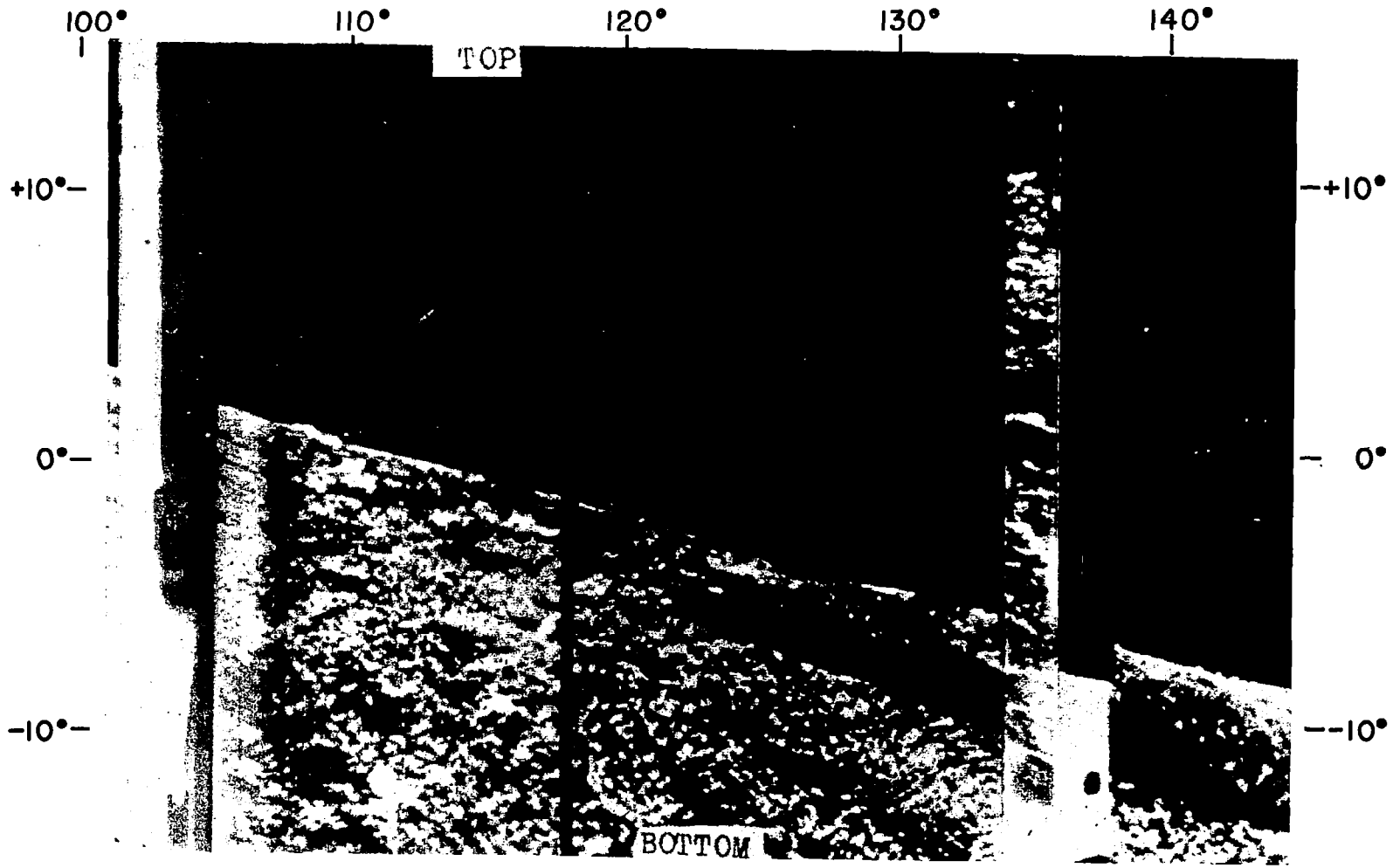

FIGURE 15. FRAME G_1

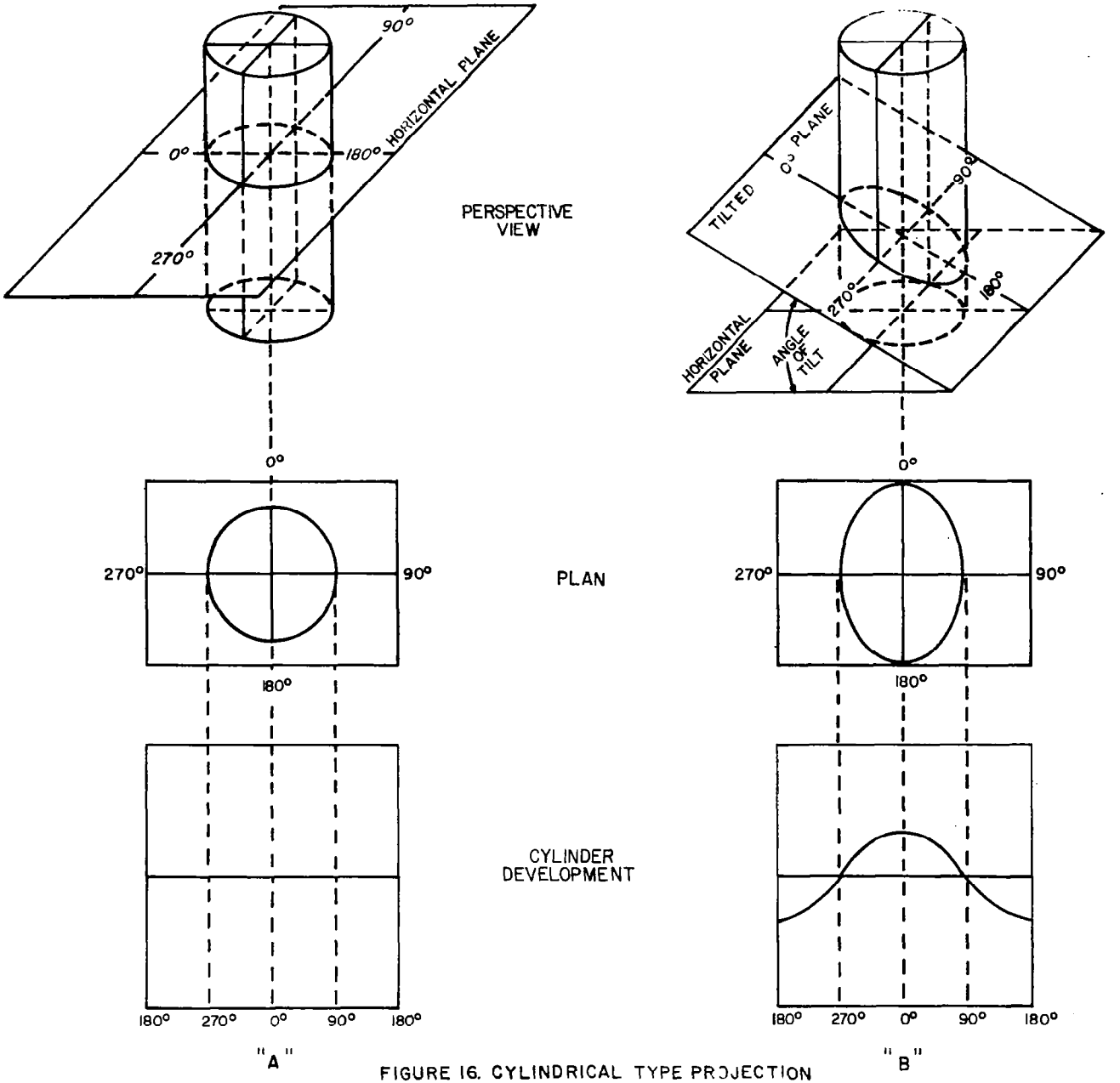

FIGURE 16. CYLINDRICAL TYPE PROJECTION

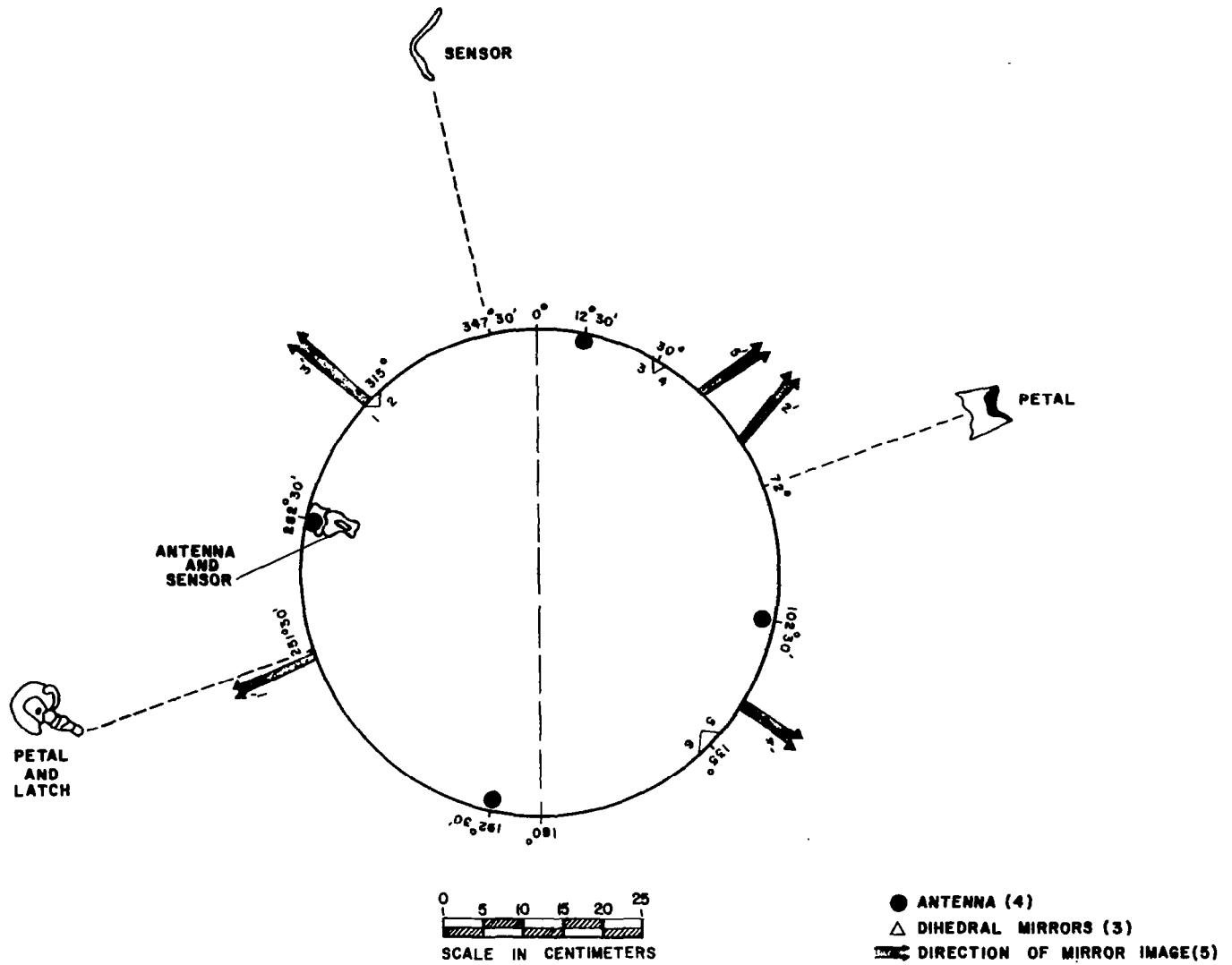

FIGURE 17. PLAN VIEW OF CAMERA INSTRUMENTATION

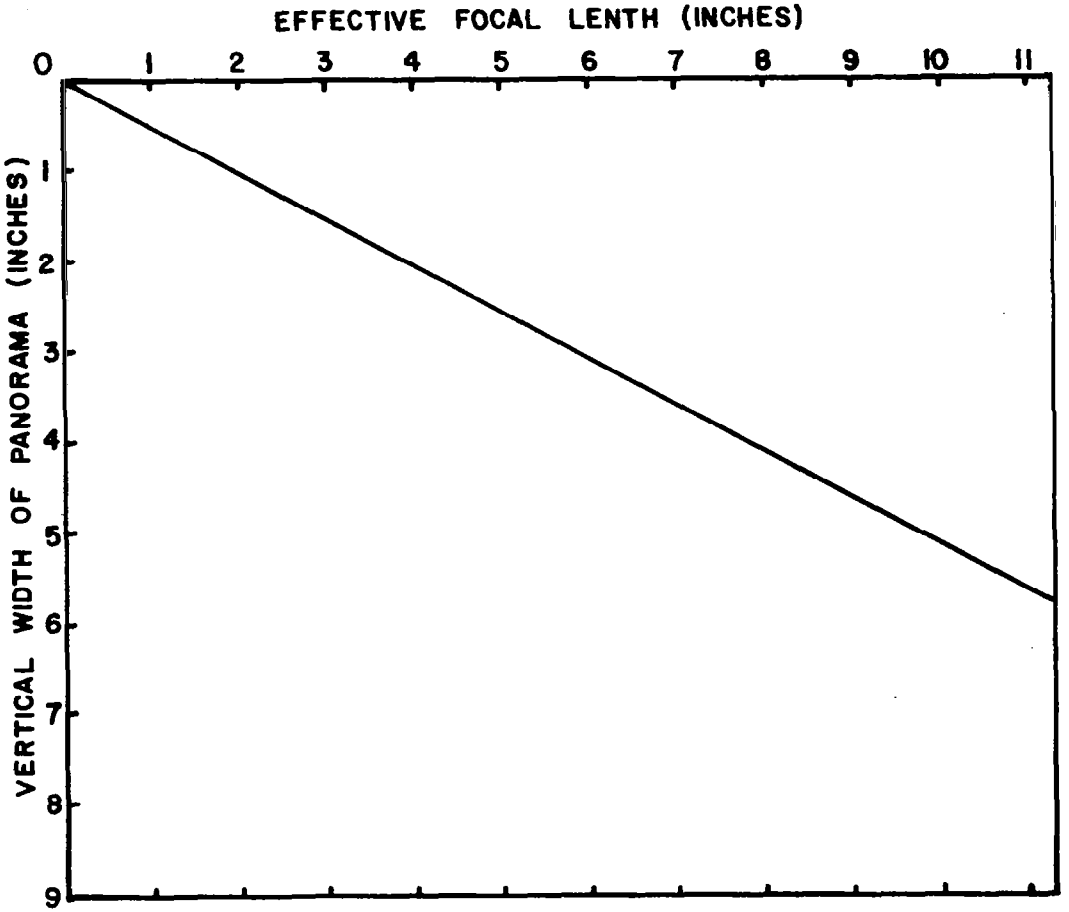

FIGURE 18. EFFECTIVE FOCAL LENGTH VS. IMAGE WIDTH

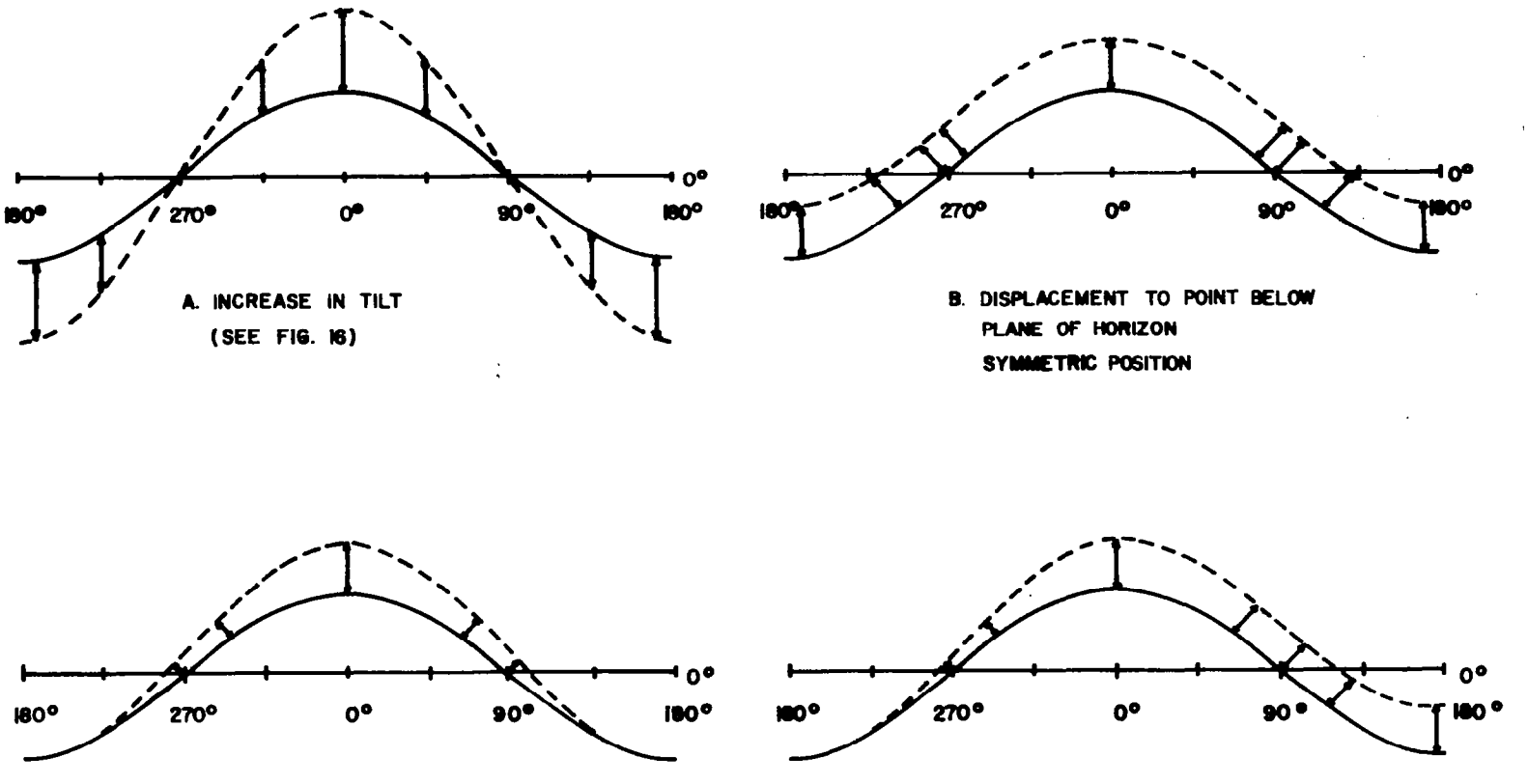

A. INCREASE IN TILT
(SEE FIG. 16)

B. DISPLACEMENT TO POINT BELOW
PLANE OF HORIZON
SYMMETRIC POSITION

C. DISPLACEMENT BELOW THE
HORIZON PLANE
ASSYMMETRIC POSITION
TILT PLANE THROUGH CENTER

D. ASSYMMETRIC TILT

FIG. 19

CONDITIONS AFFECTING THE HORIZON CURVE: SOLID LINES ARE INITIAL CURVES FOR A GIVEN TILT ANGLE; DASHED LINES ARE MODIFIED CURVES; ARROWS SHOW DIRECTION OF DISPLACEMENT.

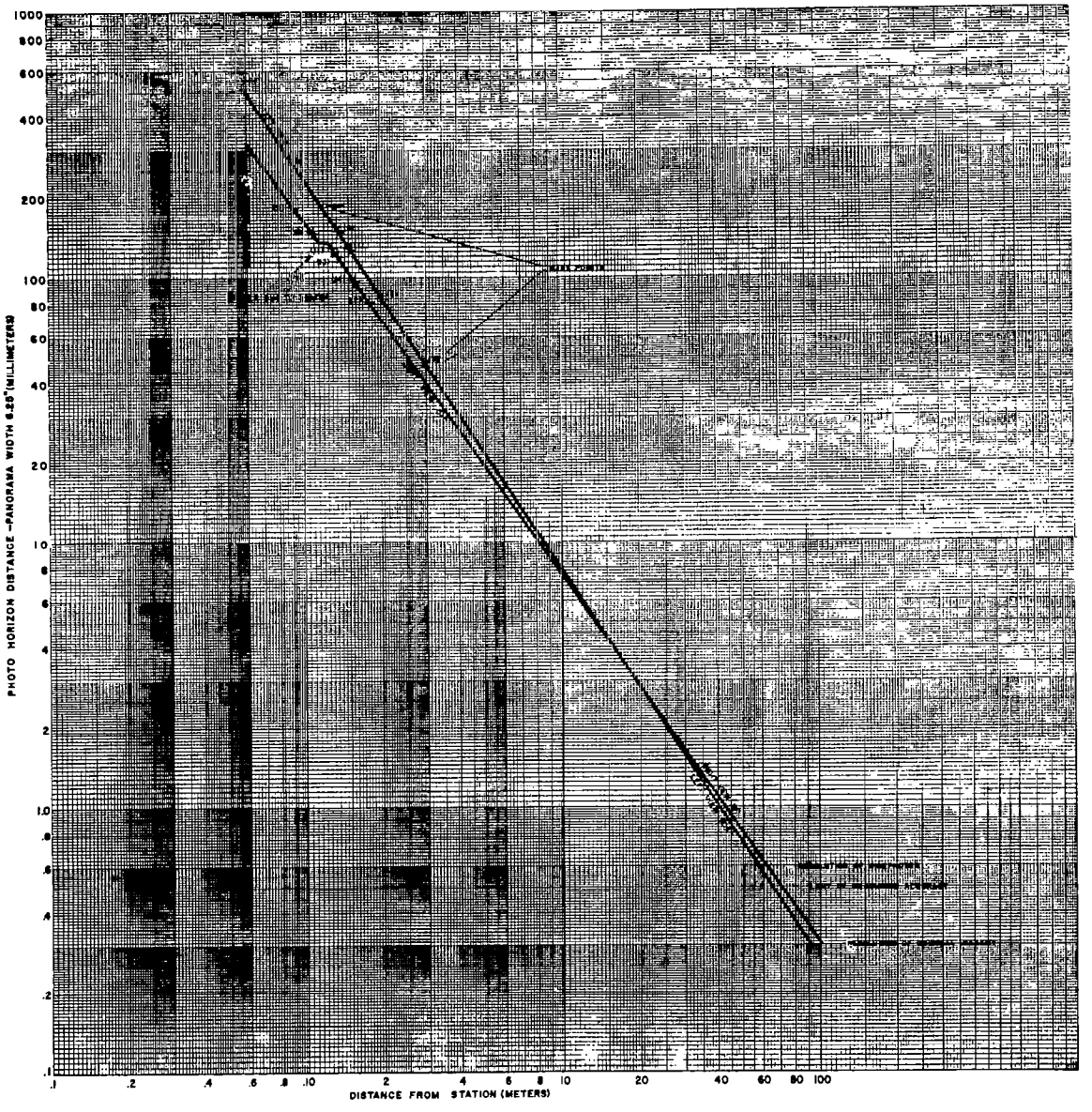

FIGURE 20. PHOTO HORIZON DISTANCE VS. GROUND DISTANCE

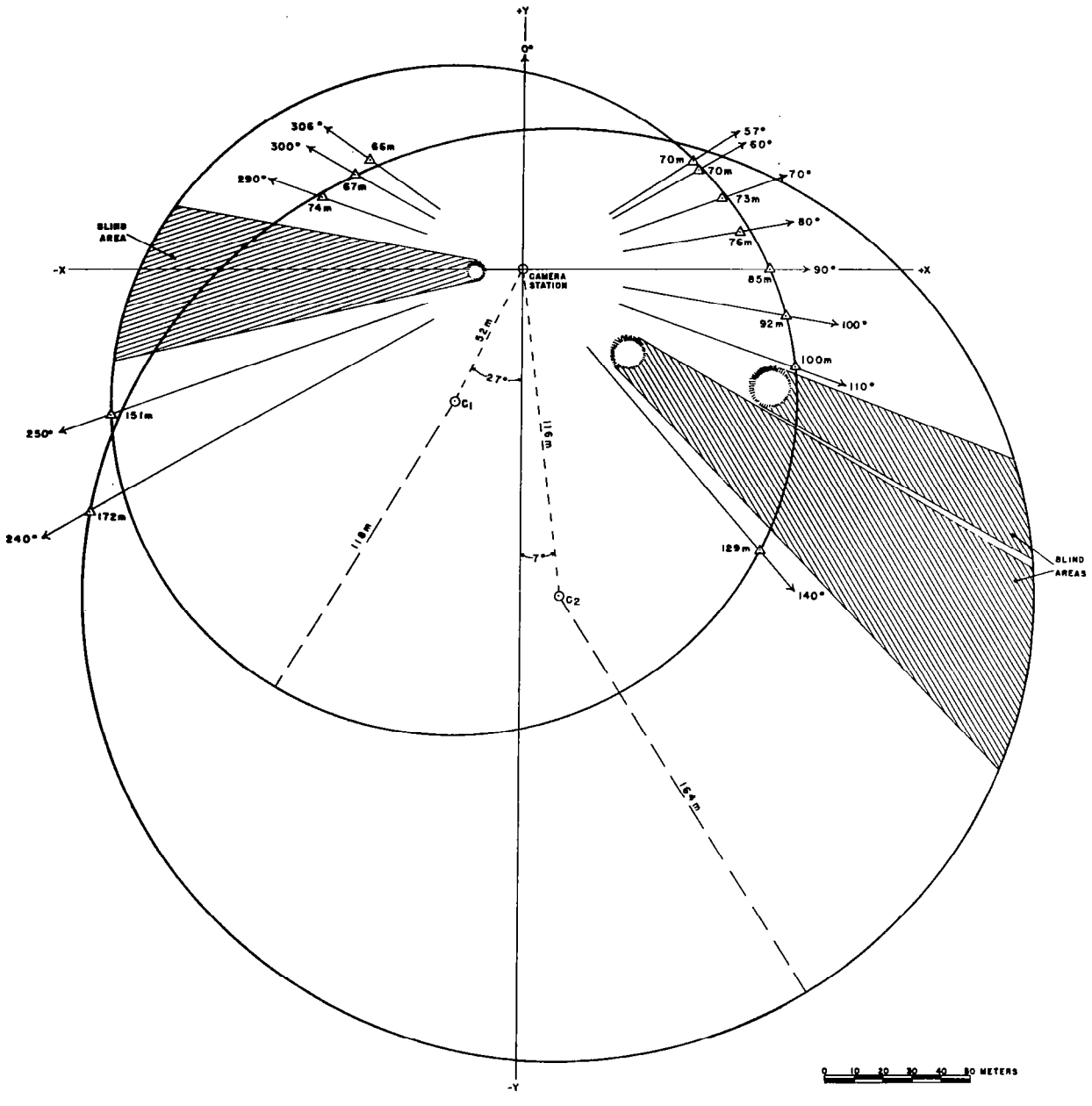

FIGURE 21. PLAN VIEW OF HORIZON DISTANCES

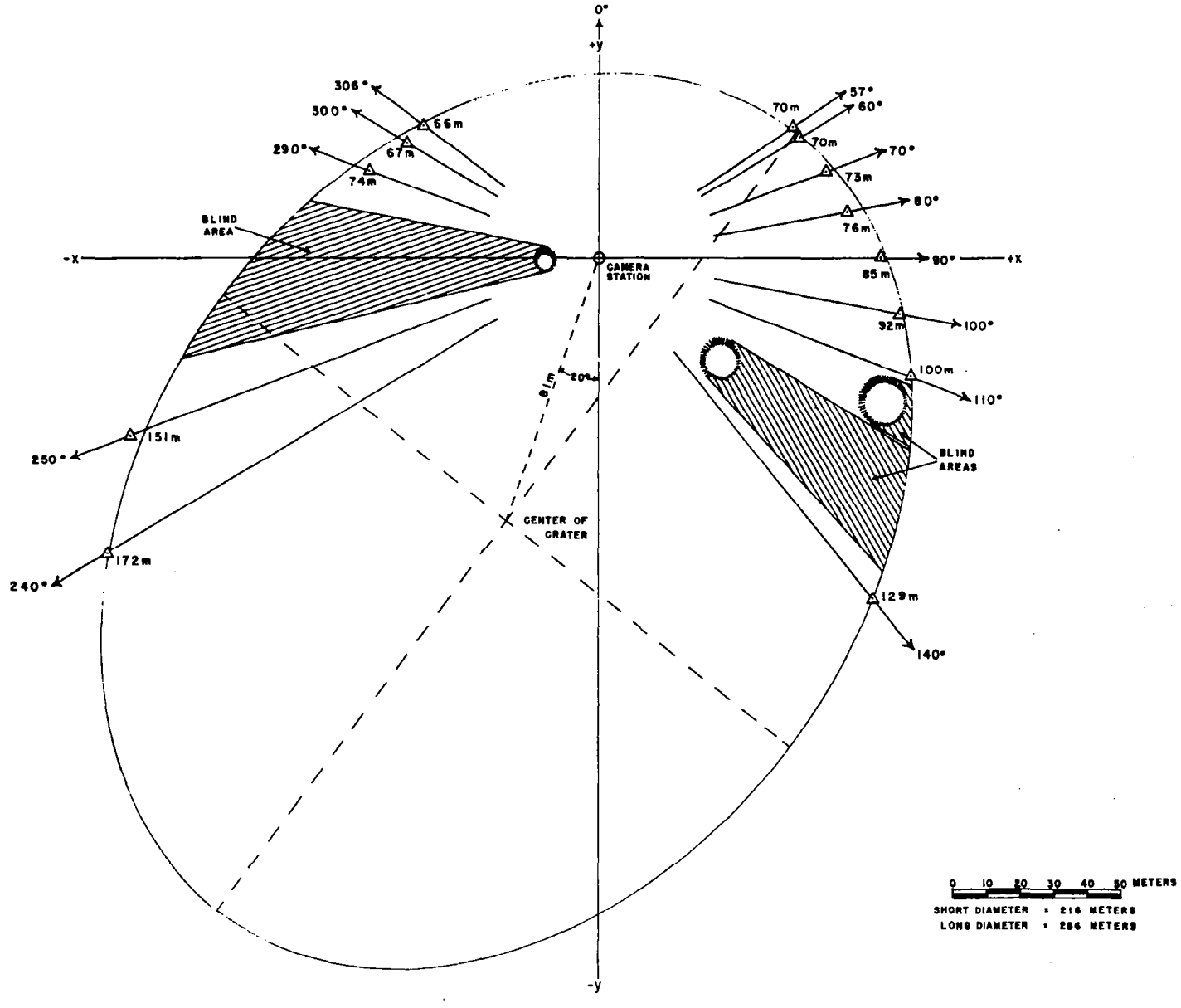

FIGURE 22. PLAN VIEW OF CRATER RIM MEASUREMENTS

FIGURE 23

SKETCH SHOWING GEOMETRIC RELATIONS OF DIHEDRAL MIRROR (SEE TEXT)

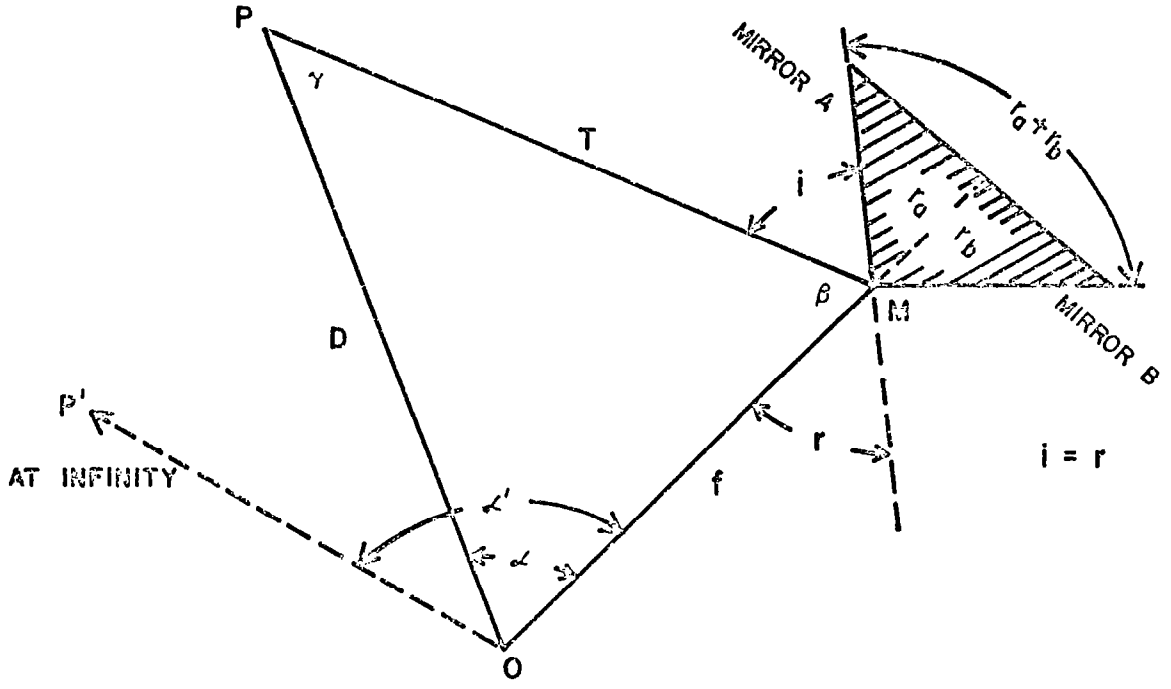

M = EDGE OF DIHEDRAL MIRROR

O = CAMERA OPTICAL CENTER

P' = POINT ON LUNAR HORIZON

P = POINT ON LUNAR SURFACE

f = RADIAL DISTANCE OF PANORAMA (FOCAL DISTANCE)

D = DISTANCE FROM O TO P

T = DISTANCE FROM P TO M

α' = AZIMUTH ANGLE TO POINT ON HORIZON ($\alpha = \angle$ FROM IMAGE)

β = CENTRAL REFLECTING ANGLE

γ = ANGLE AT P SUBTENDED BY f

i = ANGLE OF INCIDENCE

r = ANGLE OF REFLECTANCE

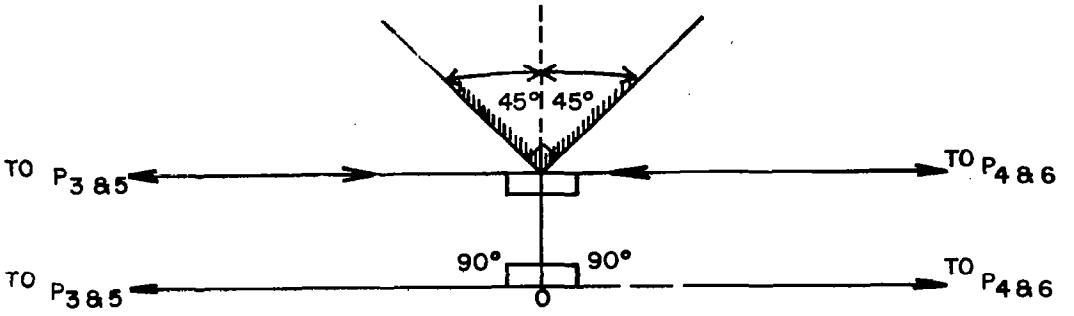

A. SECOND & THIRD DIHEDRAL PAIR

DIAGRAMS ILLUSTRATING ORIENTATION OF MIRRORS ON LUNA 9 WITH RESPECT TO THE OPTICAL CENTER AND RADIUS.
O: OPTICAL CENTER; P_n: POINT ON HORIZON

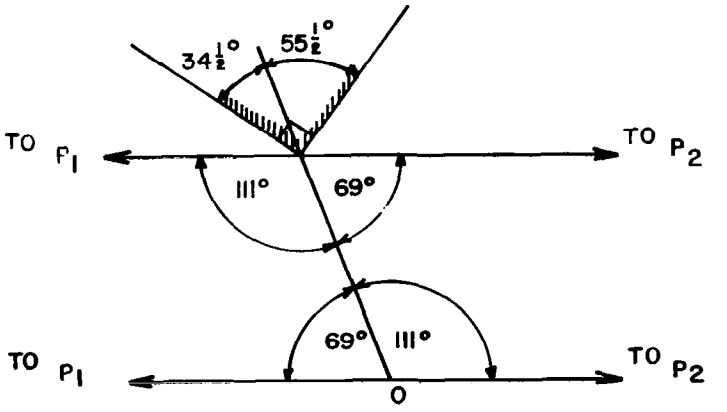

B. FIRST DIHEDRAL PAIR

FIGURE 24. ORIENTATION OF LUNA 9 MIRRORS

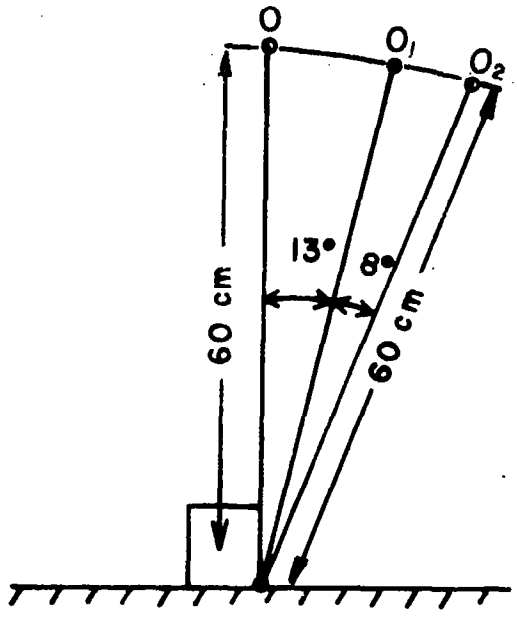

8° = 0.140 RADIANS

DISTANCE $O_1 O_2$ = 0.14 x 60 cm = 8.4 cm

FIGURE 25. DIAGRAM SHOWING DISPLACEMENT OF CAMERA CENTER WITH TILT.

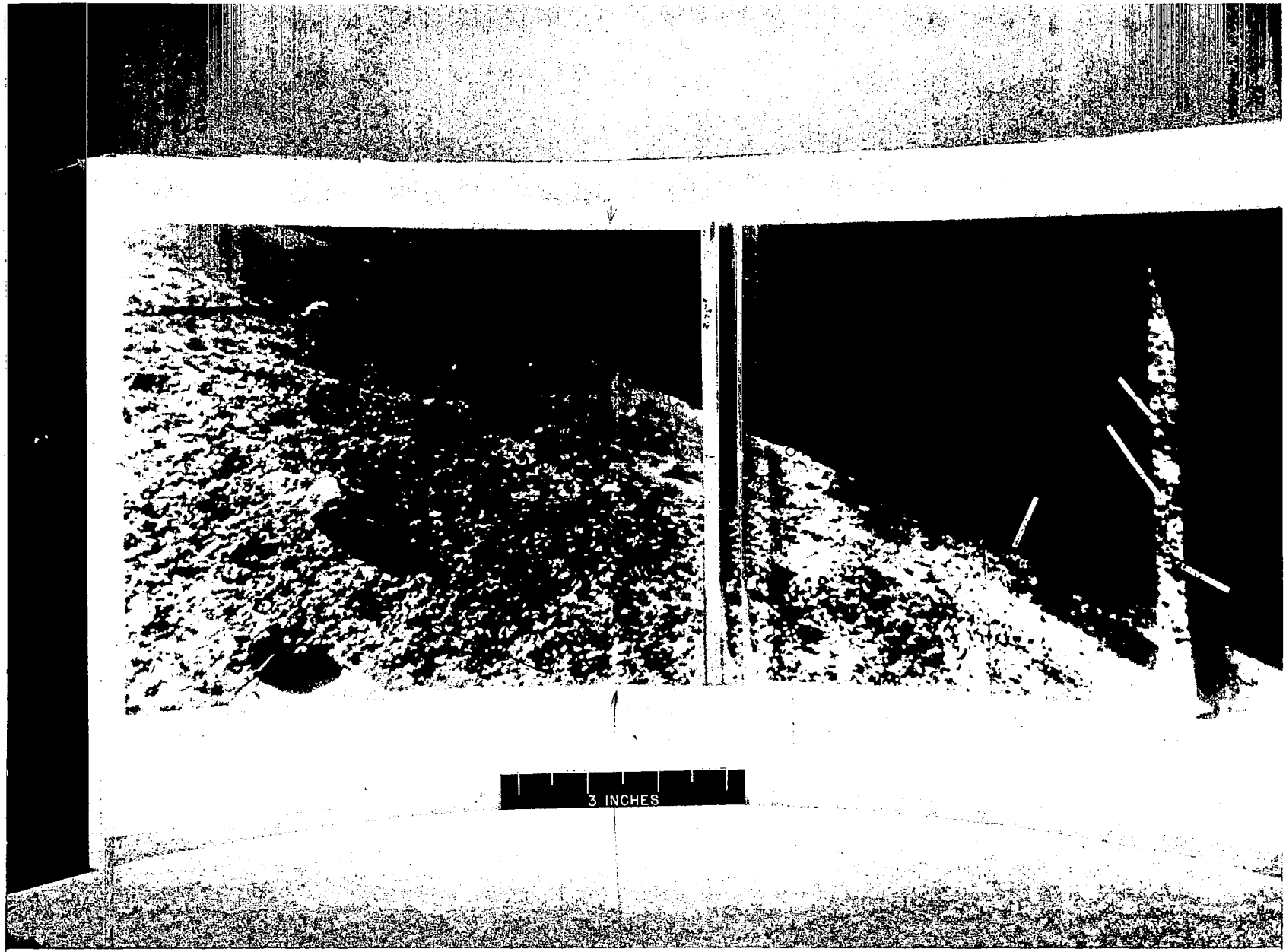

FIGURE 26. RECTIFIED IMAGES USED IN STERO PLOTTING

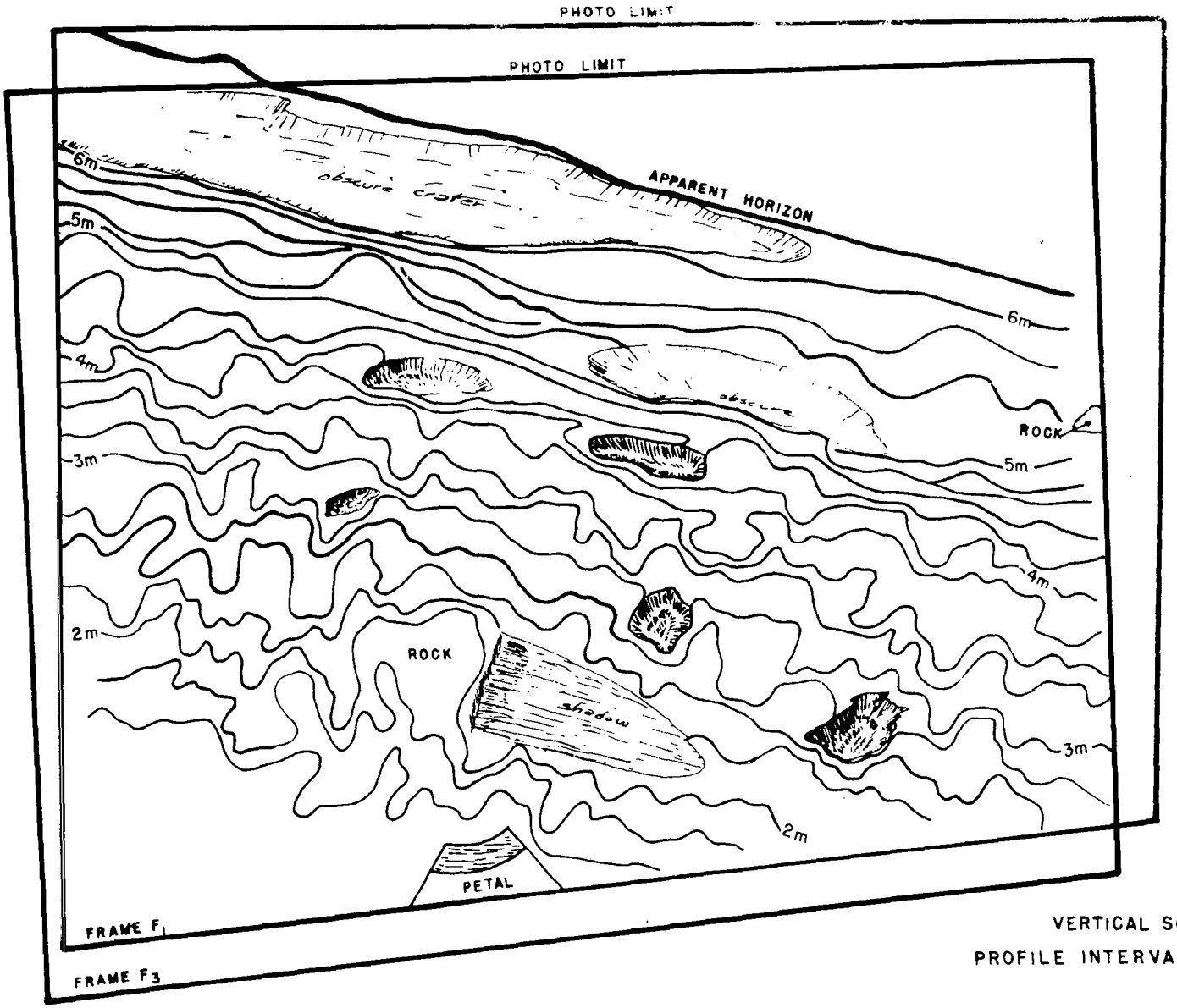

FIGURE 27. VERTICAL PROFILES PLOTTED FROM RECTIFIED IMAGERY

FIGURE 28. CUMULATIVE CURVE OF COARSE ROCK PARTICLES IN FRAME F_3

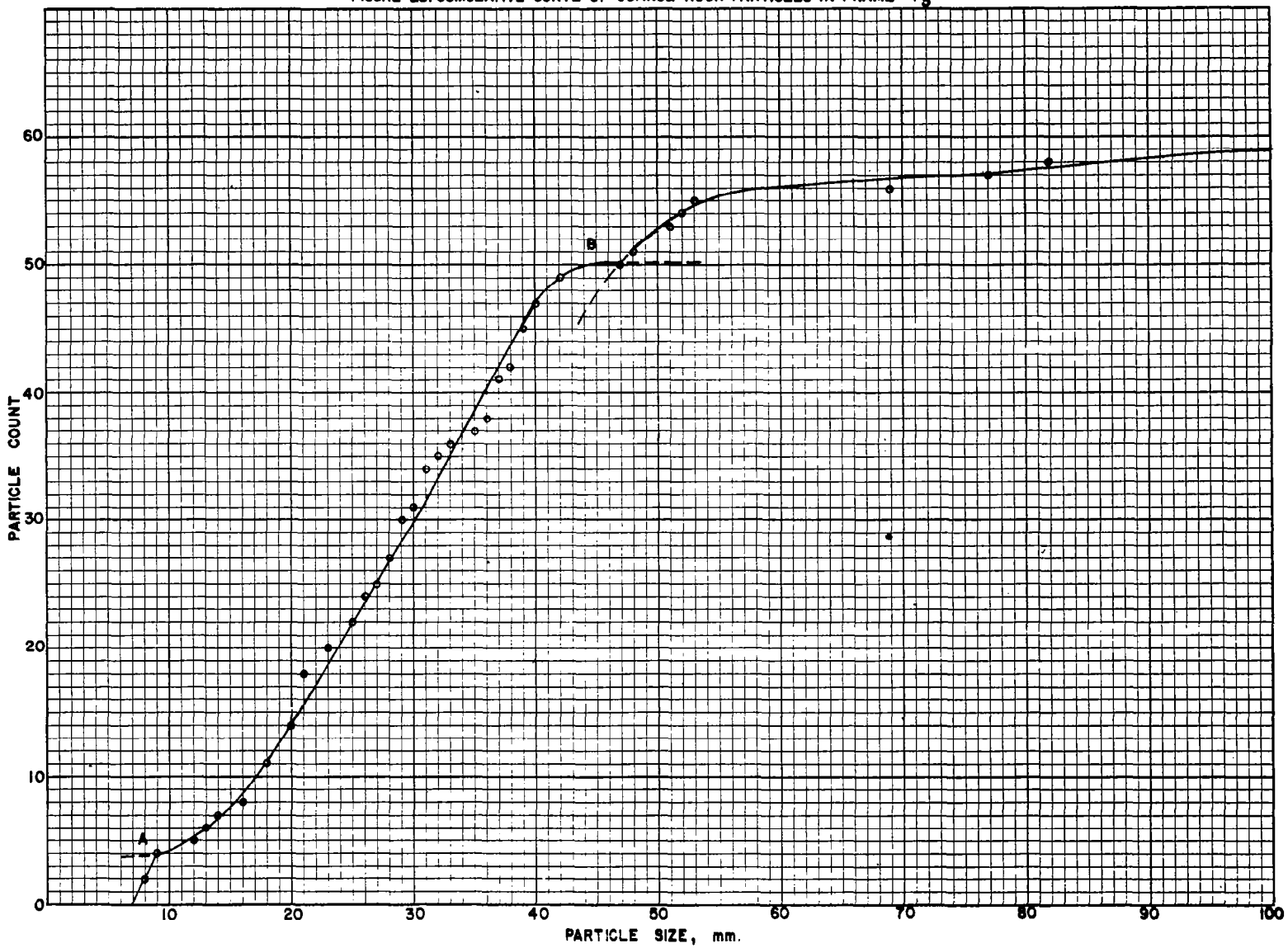

FIGURE 29. PARTICLE SIZE DISTRIBUTION OF FRAME F_3

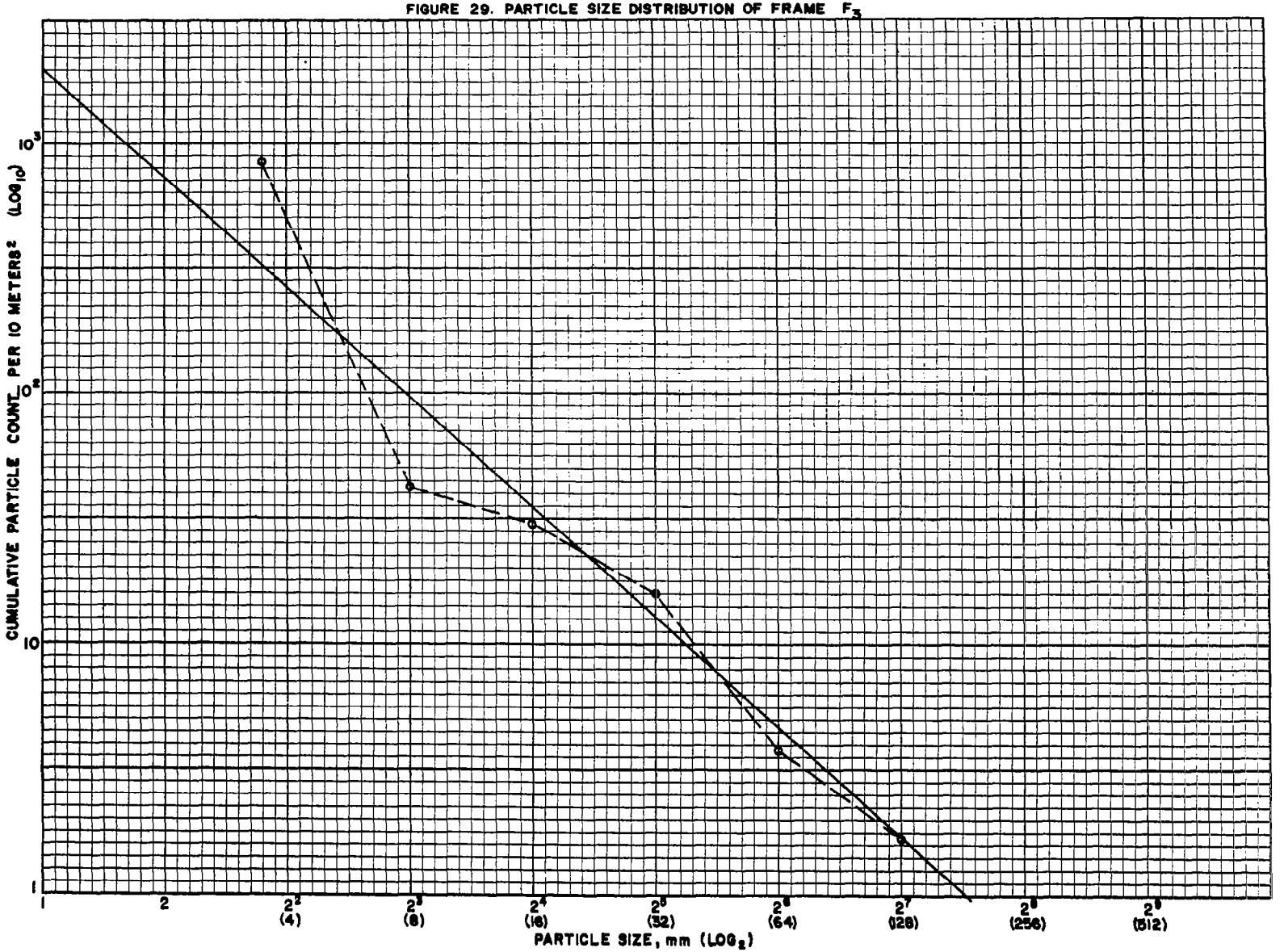

FIGURE 30

HISTOGRAMS OF CRATER COUNTS
OF LUNA 9 PANORAMA NO. 3

A. AREA FROM 0.5–2.0 METERS; AREA 3 METERS^2
B. " " 2.0–5.0 " ; " 37 "
C. " " 5.0–30.0 " ; " 940 "
D. CUMULATIVE FOR WHOLE AREA 0.5–30 METERS
TOTAL AREA 980 METERS^2

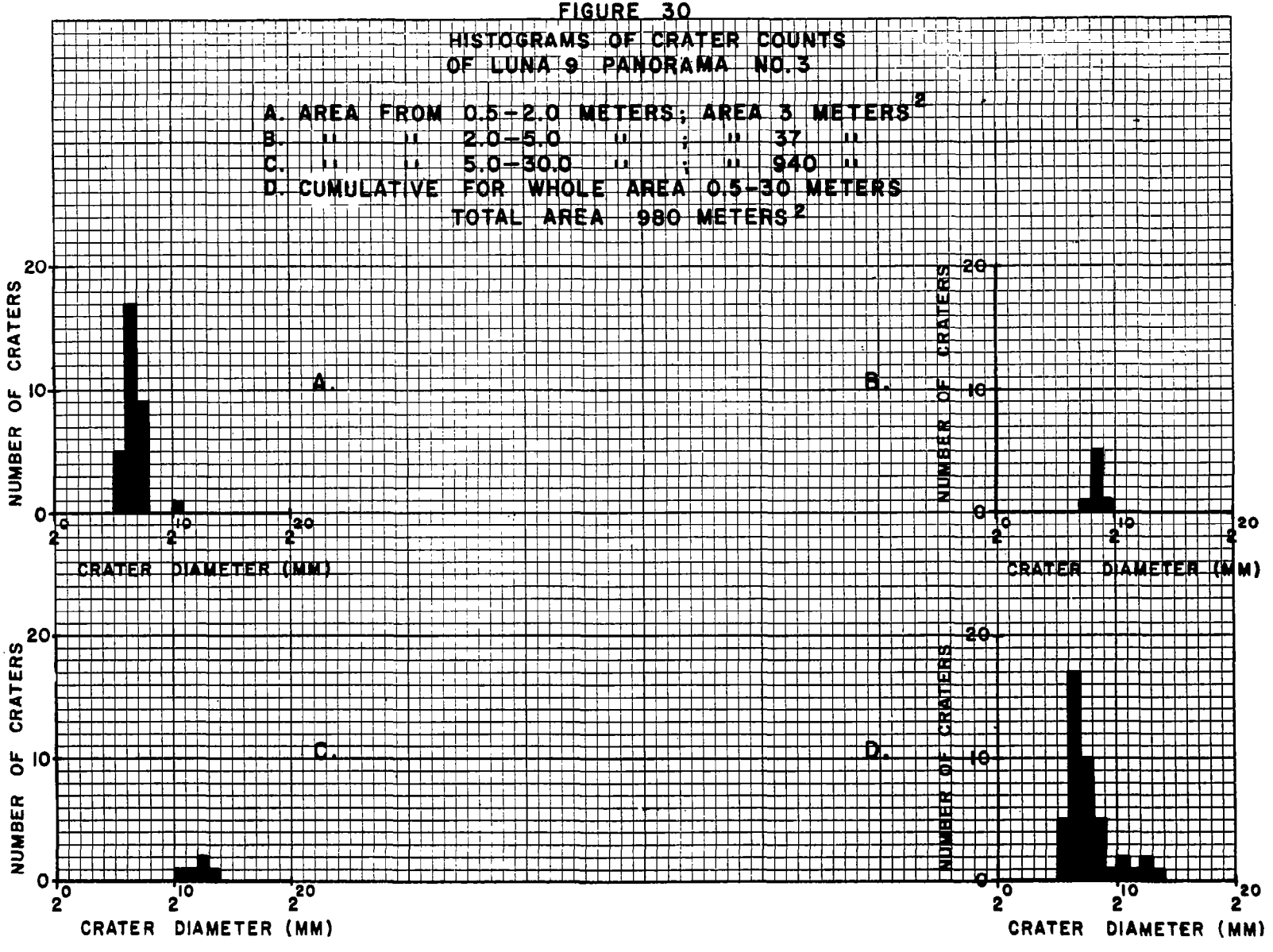

FIGURE 31
CRATER SIZE DISTRIBUTION OF
LUNA 9 PANORAMA NO. 3